Electrochimica Acta 388 (2021) 138634

Contents lists available at ScienceDirect

Electrochimica Acta

journal homepage: www.elsevier.com/locate/electacta

Semi-empirical treatment of ionophore-assisted ion-transfers in ultrathin membranes coupled to a redox conducting polymer

Yujie Liu, Gaston A. Crespo, Maria Cuartero*

Department of Chemistry, School of Engineering Sciences in Chemistry, Biotechnology and Health, KTH Royal Institute of Technology, Teknikringen 30, SE-100 44, Stockholm, Sweden

ARTICLE INFO

Article history:
Received 26 February 2021
Revised 13 April 2021
Accepted 15 May 2021
Available online 21 May 2021

keywords:
Ultrathin ion-selective membranes
Ion transfer
Charge transfer
Spectroelectrochemistry
Ion-ionophore interactions

ABSTRACT

Applying spectroelectrochemistry to all-solid-state electrodes composed of poly(3-octylthiophene) (POT) and an ultrathin ion-selective membrane on top, it is possible to monitor the dynamic charge transfer (CT) in POT when this event is coupled to ion transfers (ITs) promoted by the absence/presence of a selective ionophore in the membrane. Herein, we report on a combination of empirical and theoretical evidence revealing that different molar ratios of the ionophore and the cation exchanger in the membrane result in the modulation of non-assisted and assisted ITs of different stoichiometries. This occurs upon the same anodic voltammetric scan. The use of the developed theory together with Sigmoidal–Boltzmann fittings of the experimental dynamic absorbance observed in the POT film permits calculating voltammograms with different ITs. An easy semi-empirical treatment additionally provides the calculation of binding constants related to the assisted transfers. Furthermore, the approach is suitable for both preferred and non-preferred ions by the ionophore, which additionally leads to the estimation of the selectivity profile of the POT-membrane system. The extra discovery about the number of electrons associated to the CT in the POT film is expected to propitiate further research towards maximizing peak resolution in the voltammetric experiments. In this context, the developed theory would help in future steps towards the prediction of voltammetric responses for multi-ionophore membranes backside contacted with new redox materials, prospecting hence new electrodes for multi-ion detection with optimized analytical features.

1. Introduction

Within the field of potentiometric ion-selective electrodes (ISEs), today efforts are focused on the so-called all-solid-state configuration, which is primarily based on two key elements: the ion-to-electron transducer and ion-selective membrane (ISM) [1]. This class of ISEs has demonstrated to be the analytical technique *per excellence* for ion sensing in decentralized applications, particularly involving wearable sensors in the form of epidermal patches and microneedles as well as environmental probes for water monitoring [2–4]. The versatility, simplicity and cost-effectiveness of the fabrication process of all-solid-state potentiometric ISEs place them as a unique platform to design any gadget for ion sensing purposes. For example, a common cloth, paper or rubber material of any size and shape can be converted into an ISE through hand-made deposition of the ion-to-electron transducer (e.g., carbon nanotube ink) and then the ISM on top [5–8].

In general terms, the potentiometry readout represents the difference between the potential occurring at the ISM-sample interface and that provided by a reference electrode (RE) at zero current conditions [1]. This is specifically called 'the membrane potential' and is defined by the local equilibrium of ions present in both the ISM and sample; thus, any change in the activity of these ions results in a change in the membrane potential value. Ideally, the potential related to each interface contained in the ISE-sample-RE system should be constant, except for the membrane potential. Also, the ISE is designed in such a way that the membrane potential exclusively depends on the ion activity in the sample. As a result, the potentiometric response unequivocally follows the Nernst equation [9].

Despite potentiometric ISEs being a well-entrenched technique for ion sensing, yet not all the analytical scenarios can be addressed because of some restrictions in the analytical performance (such as the limit of detection and selectivity). Indeed, authors in

* Corresponding author.
E-mail address: mariacb@kth.se (M. Cuartero).

https://doi.org/10.1016/j.electacta.2021.138634

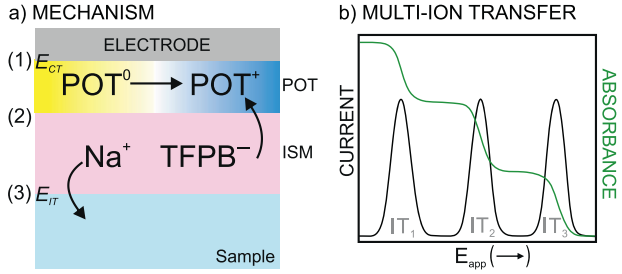

Fig. 1. (a) Illustration of the mechanism underlaying the POT-membrane system upon application of a linear sweep potential. POT^0/POT^+=neutral and oxidized poly(3-octylthiophene). Na^+TFPB^-=the cation exchanger sodium tetrakis[3,5-bis-(trifluoromethyl)phenyl]borate. ISM=ion-selective membrane. E_{CT}=charge-transfer potential. E_{IT}=ion-transfer potential. (1), (2) and (3) refer to the Electrode-POT, POT-ISM and ISM-sample interface respectively, with the electrode specifically being an ITO glass in this work. (b) Illustration of the voltammogram observed when three ion transfers (IT_1, IT_2 and IT_3) occur at the membrane-sample interface and the simultaneous dynamic absorbance recorded by spectroelectrochemistry setup. E_{app}=applied potential.

the field have directed their investigations over the last decades towards: (i) searching for new ion-to-electron transducer materials to assure the potential stability at its interface with the ISM [10–12] or (ii) even introducing an instrumental adjustment for this purpose [13]; (iii) the control of inconvenient ion fluxes across the membrane that may deteriorate the ISE response [14–16]; and (iv) discovering new ionophores with special emphasis on anions [17–19], among other actions. Of particular interest is the interrogation of ISEs with dynamic electrochemistry rather than traditional measurements at zero current conditions [20].

While the role of the ion-to-electron transducer is providing a constant potential at its interface with the ISM in classical potentiometric all-solid-state ISEs [1], extraordinary properties can be manifested when the redox state of the transducer is externally adjusted in order to control any ion-transfer (IT) process at the membrane-sample interface. Investigations pioneering this idea were based on a ISM backside contacted with a conducting polymer such as poly(3,4-ethylenedioxythiophene) (PEDOT) or poly(3-octylthiophene) (POT) [21–23]. The application of a linear sweep potential generates the oxidation or reduction of the conducting polymer and this results in a net flux of ions at the ISM-sample interface driven by electroneutrality maintenance. In the particular case of a membrane based on a cation exchanger (Na^+R^-) with a POT underlayer, POT is gradually oxidized to POT^+ and stabilized by R^- in the membrane, thus resulting in the release of Na^+ to the solution (Fig. 1a) [22]. This IT at the membrane-sample interface generates a voltametric peak whose position and current magnitude (or charge) depends on the type of ion and its concentration in the sample solution [24,25,26].

A rather wide plethora of possibilities has been recently opened around this concept, primarily involving: (i) the use of different redox materials to induce the charge disbalance in the system (such as 7,7,8,8-tetracyanoquinodimethane [24,27], self-assembled monolayers [28,29] and redox probes directly dissolved in the membrane [30–33]; (ii) the tuning of the membrane thickness and its composition (e.g., multi-ionophore nanometer-sized membranes [34,35], reduced ion-exchange capacity [36]); (iii) the electrochemical protocol (cyclic voltammetry [22,25], stripping voltammetry [37,38] or chronoamperometry [39]); and (iv) the theoretical understanding and modelling of the working mechanism.[25,26,40–43] Regarding this latter, the approach that seems to be most widely investigated (and probably accepted) in the literature refers to the definition of the applied potential as the sum of interconnected charge transfer (CT) in the redox material and IT process at the membrane-sample interface; whereas the current is assumed constant at each point of the system [25,26,42,43]. Recent directions agree in claiming that the appropriate definition of the CT, in terms of the amount of the material that is oxidized or reduced with the applied potential, is crucial to define the current observed for the system; but also for the characterization of thermodynamic aspects related to the interconnected ITs [42–44].

In our recent publication, we have introduced a new spectroelectrochemistry approach for the monitoring of the dynamic oxidation degree in the POT layer when connected to ultrathin membranes able to provide IT(s) of different nature and number [43]. The absorbance of the POT layer changes upon polarization to POT^+ (see Fig. 1a) and we could mathematically model how the POT experimentally becomes oxidized depending on the linked ITs. More specifically, the CT is expressed in a sigmoid coinciding with the range of the applied potential in which any voltametric peak occurs and with the peak potential coinciding with the inflection point of the CT curve. Whether more than one IT is possible, the entire sigmoid curve is divided into portions linked to each IT. For example, for a membrane based on three different selective receptors and thus providing three ITs, three sigmoidal portions appeared (Fig. 1b). One important finding is that, between the different ITs, the experiments and theory demonstrated that no POT is oxidized because no IT occurs [43]. This pointed out the unequivocally link between the CT and any IT process at the sample-membrane interface, but also revealed that the sigmoidal shape was not ascribed to the optical readout *per se* but to the pure CT process in POT, i.e., the integral current for the CT-IT system.

In this work, we demonstrate for the first time spectroelectrochemistry measurements to monitor the CT in POT films that are interconnected with ultrathin membranes designed to provide non-assisted (NAS) and ionophore-assisted (AS) ITs during the same polarization (voltammetric) scan. The theoretical description of how the CT advances with the applied potential reveals a huge potential of this approach for different purposes. First, the molar ratio between the ionophore and the cation exchanger in the membrane crucially dictates the nature of the IT(s) (ionophore-AS *versus* NAS ITs) that are visualized upon POT oxidation to POT^+. Second, this is the first time that both the dynamic CT and voltammograms can be predicted by knowing some initial parameters related to the ion-ionophore interaction(s) in the membrane. Finally, the theoretical model can be used in the direction to easily obtain ion-ionophore binding constants and selectivity coefficients.

2. Experimental section

2.1. Reagents, materials and equipment

Aqueous solutions were prepared by dissolving the appropriate salts in deionized water (> 18.2 MΩ). 3-octylthiophene (97%, OT), lithium perchlorate (> 98%, $LiClO_4$), high molecular weight poly(vinyl chloride) (PVC), bis(2-ethylhexyl)sebacate (DOS), sodium tetrakis[3,5-bis-(trifluoromethyl)phenyl]borate (NaTFPB), potassium ionophore I (Valinomycin), sodium ionophore X (4-tert-Butylcalix[4]arene-tetraacetic acid tetraethyl ester), sodium chloride (99.5%, NaCl), potassium chloride (99.5%, KCl), tetrahydrofuran (> 99.9%, THF) and acetonitrile (anhydrous, > 99.8%) were purchased from Sigma Aldrich. Absolute ethanol (99.5%, CH_3CH_2OH) was acquired in VWR. Indium tin oxide (ITO) coated glass slides (25 mm × 25 mm × 1.1 mm, surface resistivity 8–12 Ω/sq) were sourced from Sigma Aldrich.

Cyclic voltammetry was performed by an Autolab PGSTAT204 potentiostat (Metrohm Nordic). All the voltammograms showed in this paper are the second scan obtained in each experiment. As demonstrated in our previous publication, after discarding the very first scan, the voltammograms are very well-maintained (i.e., acceptable reproducibility) for successive scans [43].

An Autolab D/HAL light source (200–2500 nm, equipped with a software-controlled shutter) and a reflection probe (DRP-RPROBE-VIS-UV, produced by Metrohm) were used to generate illumination. Autolab Spectrophotometer UA (collecting wavelength range: 200–1100 nm), an optical cable from Dropsens (UV/VIS/NIR Optical fiber) and a lens were combined to record spectra. All instruments were controlled by Nova 2.1 software (supplied by Autolab). Calculations were accomplished in MATLAB_R2018b software.

2.2. Preparation of ITO-POT-membrane electrodes

ITO coated glass electrode was cleaned with ethanol through ultra-sonification and then rinsed with water. For the POT synthesis, a solution comprising 0.1 M of both 3-octylthiophene and $LiClO_4$ in acetonitrile (ACN) was used. After degassing by purging nitrogen for 15 min, POT was electrochemically polymerized on the ITO electrode by performing cyclic voltammetry (0–1.5 V, 100 mV/s, 2 scans) and then discharged at 0 V for 120 s. A Platinum electrode and a home-made Ag/AgCl wire were used as counter electrode (CE) and reference electrode (RE) respectively in the three-electrode cell. Thereafter, the synthesized POT film was immersed in ACN and then THF for 30 min and 10 s respectively.

Stock membrane cocktails were prepared according to the compositions presented in Table S1 (Supporting Information), essentially containing or not potassium ionophore I or sodium ionophore X. Then, the stock cocktails were diluted in THF: 50 μL of stock membrane cocktail + 150 μL of THF. A volume of 30 μL of diluted membrane cocktail was deposited on the POT-based ITO by spin coating (1500 rpm, 60 s) using a spin coater provided by GreatCell Solar (Australia).

2.3. Spectroelectrochemical measurements

The spectroelectrochemical cell was prepared as reported elsewhere [45]. Briefly, the ITO-POT-membrane electrode (working electrode, WE) is placed at the bottom of a Teflon compartment *via* a metallic piece composed of a circled window in the middle to allow the light passing. The metallic piece perfectly matches the Teflon compartment with screws. The compartment possesses the same rounded window. Next, the solution under study is added to the compartment, with the CE and RE placed inside the solution. The light source and detector are aligned to the center of the WE for the light path to come through the circled window, with the detector fixed on the bottom part of the cell and the light source introduced together with the CE and RE in the solution compartment but without touching the liquid. Thus, the POT film was illuminated from the top of the electrochemical cell and the transmitted light was collected from the bottom after absorption by the POT film. Notably, the same cell was used for the POT electropolymerization.

During CV experiments, spectra of the POT film were collected with an acquisition time of 50 ms. After discarding the very first voltammogram/spectra, four spectra were averaged to improve signal-to-noise ratio. Dynamic absorbance change of the POT film at 450 nm was selected as the optimum wavelength to distinguished between neutral and oxidized POT, as demonstrated in our recent publication [43].

3. Theory

3.1. Formal definition of interconnected CT–IT processes in POT–membrane systems

The CT–IT system is composed of a redox active film of POT that is electropolymerized on an ITO glass electrode, and the ultrathin membrane containing a fixed concentration of cation exchanger (Na^+TFPB^-) is situated on top of the POT film, as decribed in the Experimental section. Accordingly, the system has three interfaces: ITO–POT (interface 1), POT–membrane (interface 2), membrane–solution (interface 3), as illustrated in Fig. 1a. The CT occurs at the interface 1 by the application of a linear sweep potential (E_{app}), in which neutral POT is gradually oxidized to POT^+ and is doped with the $TFPB^-$ present in the membrane across the interface 2. The transport of the $TFPB^-$ at the interface 2 creates a charge disbalance in the membrane that is compensated with Na^+ (or a general cation I^+ present in the membrane) release to the solution across the interface 3, in other words, the IT process. Any IT occurring at the interface 3 may be assisted by a selective receptor (or ionophore, *L*) incorporated into the membrane.

From our previous studies with POT-membrane electrodes, we know that the $TFPB^-$ transport at the interface 2 for POT doping/undoping upon polarization has a neglected influence in the distribution of the applied potential, but also in the generated current in the system, as the membrane behaves as a true thin layer element [25,26,42].

Regarding the initial state of the POT-membrane system, while the membrane is prepared with the Na^+ cation as part of the NaTFPB cation exchanger compound, this is quickly and entirely replaced by any other cation present in the solution at relatively high concentration [25,34]. For example, for a membrane containing NaTFPB and potassium ionophore I, K^+ is expected in the membrane when this is introduced in a 10 mM KCl concentration solution. The expelled amount of Na^+ from the membrane to the solution is so tiny as compared to the bulky K^+ concentration that any voltammetric peak related to Na^+ transfer in/to the membrane is not experimentally visualized [25,34]. Accordingly, Na^+ traces in the sample solution are not considered in the development of this theory.

Then, the applied potential (E_{app}) is distributed between the CT (E_{CT}) at the interface 1 and the IT (E_{IT}) at the interface 3, and is described by Eq. (1), as proposed elsewhere [25]. The generated current upon the E_{app} is the same in all the points of the system and is provided by Eq. (2) [25], with the maximum amount of POT that can be oxidized to POT^+ equal to the amount of $TFPB^-$ in the membrane [25,26,43].

$$E_{app} = E_{CT} + E_{IT} \tag{1}$$

$$i = n_{POT} F A \partial_{POT} \frac{\partial c_{POT^+}}{\partial t} \tag{2}$$

where n_{POT} is the average number of electrons transferred in the oxidation/reduction of POT/POT^+, *F* is the Faraday constant, *A* is the area of the POT-membrane electrode that is in contact with analyte solution, ∂_{POT} is the thickness of POT film, and $\frac{\partial c_{POT^+}}{\partial t}$ is the rate of the oxidation or reduction of POT.

According to Eq. (2), it is necessary to obtain an expression defining the dynamic oxidation of POT to POT^+ to be able to calculate the current in the associated voltammograms. The next section obtains such definition in the form of analytical equations depending on the molar (or concentration) ratio $\frac{c^{org}_{L,Total}}{c^{Total}_{TFPB^-}}$ in the membrane, which was found to dictate the presence of NAS and AS ITs in our experiments (see below).

3.2. Varying the Ionophore/NaTFPB molar ratio to promote non-assisted and assisted transfer of I^+ in a sole membrane

The CT process at the interface 1 is considered as a fast process limited by electron transfer and not by the incorporation of the lipophilic anion $TFPB^-$ in the POT lattice, as above described. Therefore, the potential at this interface is assumed to be at thermodynamic equilibrium and hence the Nernst equation is used for

its description, as previously described in the literature for analogous systems [25,26]:

$$E_{CT} = E^0_{CT} - s_{POT}\ ln\frac{c_{POT^0}}{c_{POT^+}} \quad (3)$$

where E^0_{CT} is the standard potential for the CT process, s_{POT} is equal to $\frac{RT}{n_{POT}F}$ (where R is the gas constant, T is the absolute temperature, n_{POT} is the average number of electrons transferred in the oxidation or reduction of POT^0/POT^+, and F is the Faraday constant), and c_{POT^0} and c_{POT^+} are the concentrations of reduced and oxidized POT respectively.

From the total amount of POT that is electropolymerized in the ITO, only a fraction is oxidized with the applied potential. The maximum concentration of POT that can be oxidized is indeed equal to the concentration of NaTFPB that is initially present in the membrane, which is herein labeled as $c^{Total}_{TFPB^-}$. The total concentration of $TFPB^-$ will indeed be shared between the membrane and the POT lattice according to the POT^+ and POT° concentrations (c_{POT^0} *and* c_{POT^+}) through the following mass balance:

$$c^{Total}_{TFPB^-} = c_{POT^0} + c_{POT^+} \quad (4)$$

where the c_{POT^0} is equal to the $TFPB^-$ concentration that remains in the membrane (also denoted as '*org*'). Accordingly, another way to express the mass balance for the $TFPB^-$ is with Eq. (5), in which $c^{POT^+}_{TFPB} = c_{POT^+}$, as above described.

$$c^{Total}_{TFPB^-} = c^{org}_{TFPB^-} + c^{POT^+}_{TFPB^-} \quad (5)$$

Solving Eq. (4) for c_{POT^0} and inserting the result into Eq. (3), the following equation is reached:

$$E_{CT} = E^0_{CT} - s_{POT}\ \ln\left(\frac{c^{Total}_{TFPB^-} - c_{POT^+}}{c_{POT^+}}\right) \quad (6)$$

The concentration of $TFPB^-$ that is in every moment in the membrane (*org*) upon the E_{app} is in turn equal to the concentration of I^+ in the membrane according to the electroneutrality condition, and being I^+ complexed or not by the ionophore (L):

$$c^{org}_{TFPB^-} = c^{org}_{I^+} + c^{org}_{I^+-L} \quad (7)$$

Inserting Eq. (7) in Eq. (5), and considering that the concentration of oxidized POT^+ is equal to the concentration of $TFPB^-$ in its lattice $c^{POT^+}_{TFPB} = c_{POT^+}$ at every time during the E_{app}, Eq. (8) is reached:

$$c^{Total}_{TFPB^-} = c^{org}_{I^+} + c^{org}_{I^+-L} + c_{POT^+} \quad (8)$$

Solving Eq. (8) for the concentration of I^+ in the membrane ($c^{org}_{I^+}$):

$$c^{org}_{I^+} = c^{Total}_{TFPB^-} - c^{org}_{I^+-L} - c_{POT^+} \quad (9)$$

When the IT process for I^+ at the interface 3 is a NAS event, the Nernst equation is used to describe the IT as follows [25]:

$$(E_{IT})_{NAS} = (E^0_{IT})_{NAS} - s_{NAS}\ \ln\left(\frac{c^{org}_{I^+}}{c^{aq}_{I^+}}\right) \quad (10)$$

where $(E^0_{IT})_{NAS}$ is the standard potential for the NAS IT, s_{NAS} is equal to $\frac{RT}{n_{NAS}F}$ (with n_{NAS} being the number of I^+ transferred at the membrane-solution interface for the NAS IT event) and $c^{aq}_{I^+}$ is the concentration of I^+ in the sample solution.

Inserting Eqs. (6) and (10) into Eq. (1), the applied potential (E_{app}) related to the NAS transfer of I^+ is described by Eq. (11):

$$E_{app} = E^0_{CT} - s_{POT}\ \ln\left(\frac{c^{Total}_{TFPB^-} - c_{POT^+}}{c_{POT^+}}\right) + (E^0_{IT})_{NAS} - s_{NAS}\ \ln\left(\frac{c^{org}_{I^+}}{c^{aq}_{I^+}}\right) \quad (11)$$

Then, Eq. (12) is reached by inserting Eq. (9) into Eq. (11), considering that s_{POT} and s_{NAS} are ideally equal because n_{POT} has to be equal to n_{NAS} to assure electroneutrality in the system, and reorganizing:

$$\left(\frac{c_{POT^+}}{c^{Total}_{TFPB^-}}\right)^2 + \left[\frac{c^{org}_{I^+-L}}{c^{Total}_{TFPB^-}} - 2 - e^{\frac{E_{app} - \left(E^0_{CT} + (E^0_{IT})_{NAS}\right)}{-s_{NAS}} + \ln\left(\frac{c^{aq}_{I^+}}{c^{Total}_{TFPB^-}}\right)}\right] \times\left(\frac{c_{POT^+}}{c^{Total}_{TFPB^-}}\right) + \left(1 - \frac{c^{org}_{I^+-L}}{c^{Total}_{TFPB^-}}\right) = 0 \quad (12)$$

For a detailed description on how to reach Eq. (12), the reader is kindly referred to the Supporting Information.

Rewriting Eq. (12) by solving it for the term $\frac{c_{POT^+}}{c^{Total}_{TFPB^-}}$ as a function of E_{app}, Eq. (13) is obtained:

$$\frac{c_{POT^+}}{c^{Total}_{TFPB^-}} = \frac{2 - B_{NAS} + e^{\frac{A_{NAS} - E_{app}}{s_{NAS}} + C_{NAS}} - \sqrt{\left(2 - B_{NAS} + e^{\frac{A_{NAS} - E_{app}}{s_{NAS}} + C_{NAS}}\right)^2 + B_{NAS} - 4}}{2} \quad (13)$$

with

$$A_{NAS} = E^0_{CT} + (E^0_{IT})_{NAS} \quad (14)$$

$$B_{NAS} = \frac{c^{org}_{I^+-L}}{c^{Total}_{TFPB^-}} \quad (15)$$

$$C_{NAS} = \ln\left(\frac{c^{aq}_{I^+}}{c^{Total}_{TFPB^-}}\right) \quad (16)$$

Notably, when the binding constant between I^+ and L is high enough, the NAS and AS ITs for I^+ will take place at different potential windows, which means that $c^{org}_{I^+-L}$ remains invariable during NAS IT process (and equal to $c^{org}_{L,T}$) and it starts decreasing when the AS IT takes place. As a result, B_{NAS} is constant, as well as A_{NAS} and C_{NAS} in the potential window of the NAS IT. Then, considering that the total amount of POT that can be oxidized to POT^+ is equal to the amount of NaTFPB initially present in the membrane, Eq. (13) represents the degree of POT (from 0 to 1) that is oxidized to POT^+ during the NAS IT process.

Considering now the AS transfer of I^+, the potential at the interface 3 (Fig. 1a) is described by the Nernst equation as follows [25]:

$$(E_{IT})_{AS} = (E^0_{IT})_{AS} - s_{AS} ln\left(\frac{c^{org}_{I^+-L}}{c^{org}_L c^{aq}_{I^+}}\right) \quad (17)$$

where $(E^0_{IT})_{AS}$ is the standard potential for the AS IT, s_{AS} is equal to $\frac{RT}{n_{AS}F}$ (with n_{AS} being the number of I^+ transferred at the membrane-solution interface for AS IT event) and c^{org}_L the concentration of free (non-complexed) ionophore L in the membrane phase.

Inserting Eqs. (17) and (10) into Eq. (1), the applied potential (E_{app}) related to the AS transfer of I^+ is described by Eq. (18):

$$E_{app} = \left[E^0_{CT} - s_{POT}\ln\left(\frac{c^{Total}_{TFPB^-} - c_{POT^+}}{c_{POT^+}}\right)\right] + \left[(E^0_{IT})_{AS} - s_{AS}\left(ln\frac{c^{org}_{I^+-L}}{c^{org}_L c^{aq}_{I^+}}\right)\right] \quad (18)$$

The total concentration of L in the membrane $c^{org}_{L,Total}$ is distributed as free L (c^{org}_L) and complexed I^+–L ($c^{org}_{I^+-L}$) as follows:

$$c^{org}_{L,Total} = c^{org}_L + c^{org}_{I^+-L} \quad (19)$$

Solving Eq. (19) for c_L^{org}:

$$c_L^{org} = c_{L,Total}^{org} - c_{I^+-L}^{org} \tag{20}$$

And solving Eq. (8) for $c_{I^+-L}^{org}$:

$$c_{I^+-L}^{org} = c_{TFPB^-}^{Total} - c_{I^+}^{org} - c_{POT^+} \tag{21}$$

This latter equation is rearranged into Eq. (22), assuming that the NAS and AS transfers of I^+ occur in totally separated potential windows and hence, the NAS IT does not take place during the AS IT process and *viceversa* (i.e., $c_{I^+}^{org} = 0$).

$$c_{I^+-L}^{org} = c_{TFPB^-}^{Total} - c_{POT^+} \tag{22}$$

Inserting then Eq. (22) into Eq. (20):

$$c_L^{org} = c_{L,Total}^{org} - c_{TFPB^-}^{Total} + c_{POT^+} \tag{23}$$

Next, Eq. (24) is obtained by inserting Eqs. (22) and (23) into Eq. (18), considering that $s_{POT} = s_{AS}$ are ideally equal since $n_{POT} = n_{NAS}$ to assure electroneutrality in the system, and reorganizing:

$$\left(\frac{c_{POT^+}}{c_{TFPB^-}^{Total}}\right)^2\left[e^{\frac{E_{app}-\left(E_{CT}^0+\left(E_{IT}^0\right)_{AS}\right)}{-s_{AS}}+\ln\left(c_{I^+}^{aq}\right)}-1\right] + \left(\frac{c_{POT^+}}{c_{TFPB^-}^{Total}}\right)\left\{\left(\frac{c_{L,Total}^{org}}{c_{TFPB^-}^{Total}}-1\right)\left[e^{\frac{E_{app}-\left(E_{CT}^0+\left(E_{IT}^0\right)_{AS}\right)}{-s_{AS}}+\ln\left(c_{I^+}^{aq}\right)}\right]+2\right\}-1=0 \tag{24}$$

For a detailed description on how to reach Eq. (24), the reader is kindly referred to the Supporting Information.

Rewriting Eq. (24) by solving it for $\frac{c_{POT^+}}{c_{TFPB^-}^{Total}}$ as a function of E_{app}, Eq. (25) is obtained:

$$\frac{c_{POT^+}}{c_{TFPB^-}^{Total}} = \frac{-(B_{AS}-1)\times e^{\frac{A_{AS}-E_{app}}{s_{AS}}+C_{AS}}-2 + \sqrt{\left[(B_{AS}-1)\times e^{\frac{A_{AS}-E_{app}}{s_{AS}}+C_{AS}}+2\right]^2+4e^{\frac{A_{AS}-E_{app}}{s_{AS}}+C_{AS}}-4}}{2e^{\frac{A_{AS}-E_{app}}{s_{AS}}+C_{AS}}-2} \tag{25}$$

with

$$A_{AS} = E_{CT}^0 + (E_{IT}^0)_{AS} \tag{26}$$

$$B_{AS} = \frac{c_{L,Total}^{org}}{c_{TFPB^-}^{Total}} \tag{27}$$

$$C_{AS} = ln(c_{I^+}^{aq}) \tag{28}$$

Considering that the total amount of POT that can be oxidized to POT^+ is equal to the amount of NaTFPB initially present in the membrane, Eq. (25) represents the degree of POT that is oxidized to POT^+ during the AS IT process. Notably, A_{AS}, B_{AS} and C_{AS} are constant values, because all the implied concentrations are fixed in the experimental preparation of the ITO-POT-membrane system. In particular, the $\frac{c_{POT^+}}{c_{TFPB^-}^{Total}}$ of the AS transfer of I^+, and therefore the current as defined in Eq. (2), directly depends on the $\frac{c_{L,Total}^{org}}{c_{TFPB^-}^{Total}}$ concentration (i.e., the ionophore / NaTFPB molar ratio) in the membrane through the parameter B_{AS}. This is an important finding towards the prediction of the response of membranes formulated with different $\frac{c_{L,Total}^{org}}{c_{TFPB^-}^{Total}}$, as those explored in this paper.

3.3. Current profiles upon anodic linear sweep potential in membranes with increasing Ionophore/NaTFPB molar ratio

The current generated in the ITO-POT-membrane system has been defined by Eq. (2), which depends on the dynamic generation of POT^+ upon the experimental time. This is in turn given by the applied potential and a fixed scan rate as follows [25]:

$$E_{app} = E_{turn} + vt \tag{29}$$

with $E_{turn}$the initial potential and v is the scan rate.

Eqs. (13) and (25) can be reformulated in terms of the applied potential provided in Eq. (29), as follows (Eq. (30) and Eq. (31) respectively):

$$\left(\frac{c_{POT^+}}{c_{TFPB^-}^{Total}}\right)_{NAS} = \frac{2-B_{NAS}+e^{\frac{A_{NAS}-(E_{turn}+vt)}{s_{NAS}}+C_{NAS}} - \sqrt{\left(2-B_{NAS}+e^{\frac{A_{NAS}-(E_{turn}+vt)}{s_{NAS}}+C_{NAS}}\right)^2+B_{NAS}-4}}{2} \tag{30}$$

$$\left(\frac{c_{POT^+}}{c_{TFPB^-}^{Total}}\right)_{AS} = \frac{-(B_{AS}-1)\times e^{\frac{A_{AS}-(E_{turn}+vt)}{s_{AS}}+C_{AS}}-2 + \sqrt{\left[(B_{AS}-1)\times e^{\frac{A_{AS}-(E_{turn}+vt)}{s_{AS}}+C_{AS}}+2\right]^2+4e^{\frac{A_{AS}-(E_{turn}+vt)}{s_{AS}}+C_{AS}}-4}}{2e^{\frac{A_{AS}-(E_{turn}+vt)}{s_{AS}}+C_{AS}}-2} - \left(\frac{c_{POT^+}}{c_{TFPB^-}^{Total}}\right)_{NAS}^{Total} \tag{31}$$

Then, these two equations are combined in a unique formula that considers both the NAS and AS transfers of I^+ occurring at different potential windows during the applied linear sweep potential, Eq. (32):

$$\left(\frac{c_{POT^+}}{c_{TFPB^-}^{Total}}\right)_{NAS+AS} = \frac{2-B_{NAS}+e^{\frac{A_{NAS}-(E_{turn}+vt)}{s_{NAS}}+C_{NAS}} - \sqrt{\left(2-B_{NAS}+e^{\frac{A_{NAS}-(E_{turn}+vt)}{s_{NAS}}+C_{NAS}}\right)^2+B_{NAS}-4}}{2} + \frac{-(B_{AS}-1)\times e^{\frac{A_{AS}-(E_{turn}+vt)}{s_{AS}}+C_{AS}}-2 + \sqrt{\left[(B_{AS}-1)\times e^{\frac{A_{AS}-(E_{turn}+vt)}{s_{AS}}+C_{AS}}+2\right]^2+4e^{\frac{A_{AS}-(E_{turn}+vt)}{s_{AS}}+C_{AS}}-4}}{2e^{\frac{A_{AS}-(E_{turn}+vt)}{s_{AS}}+C_{AS}}-2} - \left(\frac{c_{POT^+}}{c_{TFPB^-}^{Total}}\right)_{NAS}^{Total} \tag{32}$$

Eq. (32) can be inserted into Eq. (2) to calculate the current upon the applied potential for membranes containing different Ionophore/NaTFPB ratios.

3.4. Estimation of logarithmic selectivity coefficients

The overall reaction occurring in the ITO-POT-ISM is described by the following equilibrium assuming one electron transfer in the CT process and the IT of I^+ as the preferred ion for the ionophore *L* [22]:

$$POT_{(POT)} + e^- + TFPB_{(m)}^- + I_{(m)}^+ \leftrightarrow POT_{(POT)}^+ + TFPB_{(POT)}^- + I_{(aq)}^+ \tag{33}$$

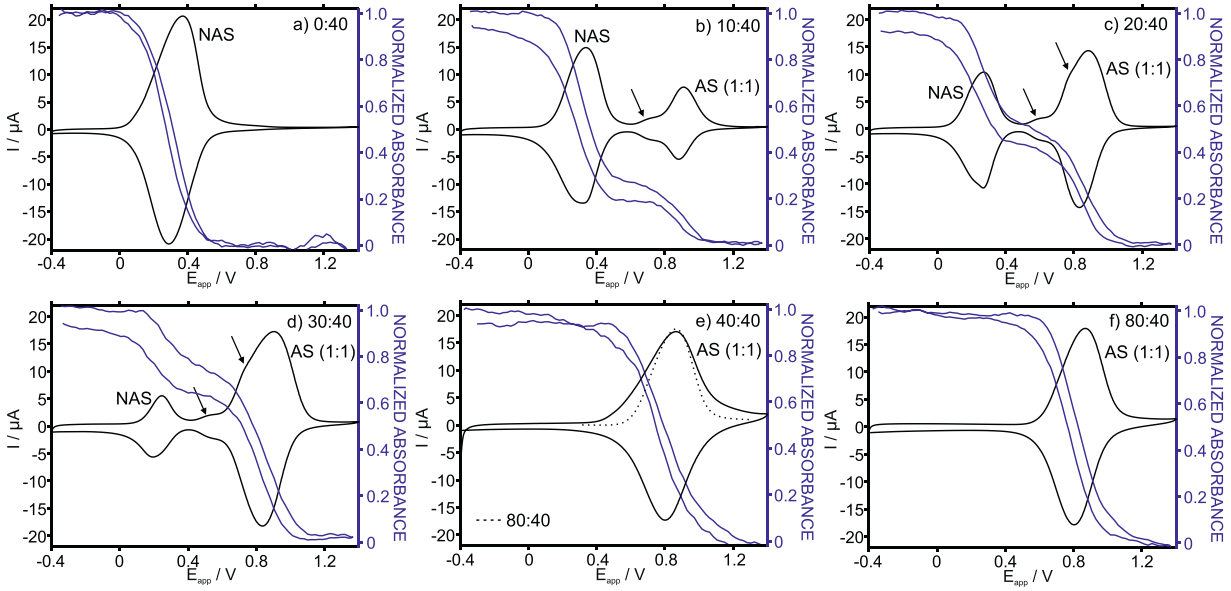

Fig. 2. Voltammograms and dynamic absorbance of the POT film observed in 10 mM KCl solution with membranes formulated with increasing potassium ionophore/NaTFPB molar ratio: **(a)** 0:40, **(b)** 10:40, **(c)** 20:40, **(d)** 30:40, **(e)** 40:40 and **(f)** 80:40. Scan rate=100 mV s^{-1}. NAS=non-assisted transfer. AS (1:1)=assisted transfer with 1:1 stoichiometry (For interpretation of the references to color in this figure, the reader is referred to the web version of this article.).

The potential related to the entire process is described by the Nernst equation according to Eq. (34):

$$E = E^0 - \frac{RT}{F}\ln\left(\frac{c_{POT^0}}{c_{POT^+}}\frac{c^{org}_{TFPB^-}}{c^{POT^+}_{TFPB^-}}\frac{c^{org}_{I^+}}{c^{aq}_{I^+}}\right) \quad (34)$$

This latter equation can be re-written as Eq. (35):

$$E = E^0 - \frac{RT}{F}\ln\frac{c_{POT^0}}{c_{POT^+}}\frac{c^{org}_{TFPB^-}}{c^{POT^+}_{TFPB^-}} - \frac{RT}{F}\ln\frac{c^{org}_{I^+}}{c^{aq}_{I^+}} \quad (35)$$

Then, considering the IT of a non-preferred cation (J^+), an analogous equation can be formulated reckon with the modulation of the selectivity coefficient ($K_{I,J}$) as per definition of the well-known Nicolskii coefficient applied to ISMs [46]:

$$E = E^0 - \frac{RT}{F}\ln\frac{c_{POT^0}}{c_{POT^+}}\frac{c^{org}_{TFPB^-}}{c^{POT^+}_{TFPB^-}} - \frac{RT}{F}\ln K_{I,J}\frac{c^{org}_{J^+}}{c^{aq}_{J^+}} \quad (36)$$

The two first terms in Eqs. (35) and (36) are constant (labelled from now on as D) and equal between them in both equations whether E is considered equal to the peak potential in the associated IT voltammogram:

$$E_{peak,I^+} = D - \frac{RT}{F}\ln\frac{c^{org}_{I^+}}{c^{aq}_{I^+}} \quad (35a)$$

$$E_{peak,\ J^+} = D - \frac{RT}{F}\ln K_{I,J}\frac{c^{org}_{J^+}}{c^{aq}_{J^+}} \quad (36a)$$

By subtracting Eqs. (35) and (36), and considering that $c^{org}_{I^+} = c^{org}_{J^+}$ in the individual IT of each cation, the following expression is obtained:

$$\log K_{I,J} = \frac{\left(E_{peak,\ J^+} - E_{peak,I^+}\right)F}{RT\ ln10} + log\frac{c^{aq}_{I^+}}{c^{aq}_{J^+}} \quad (37)$$

For the particular case that the voltammetric peak potentials are obtained at $c^{aq}_{I^+} = c^{aq}_{J^+}$, Eq. (37) is indeed simplified to:

$$\log K_{I,J} = \frac{\left(E_{peak,\ J^+} - E_{peak,I^+}\right)F}{RT\ ln10} \quad (38)$$

3.5. Estimation of ion-ionophore binding constants

Eq. (17) arising from the application of the Nernst equation to the NAS transfer of I^+ can be rewritten as Eq. (39):

$$(E_{IT})_{AS} = (E^0_{IT})_{AS} - s_{AS}ln\left(\frac{\beta_{I-L}\ c^{\ org}_{I^+}}{c^{aq}_{I^+}}\right) \quad (39)$$

with the ion-ionophore binding constant being $\beta_{I-L} = {}^{c^{org}_{I-L}}/_{c^{org}_{I^+}c^{org}_{L}}$.

By subtracting Eqs. (39) and (10) and considering that $s_{AS} = s_{NAS}$, Eq. (40) is reached. For a detailed description on how to reach Eq. (40), the reader is kindly referred to the Supporting Information.

$$(E_{IT})_{AS} - (E_{IT})_{NAS} = (E^0_{IT})_{AS} - (E^0_{IT})_{NAS} - s_{AS}ln(\beta_{I-L}\ ) \quad (40)$$

Solving Eq. (40) for β_{I-L} :

$$ln\beta_{I-L} = \frac{(E_{IT} - E^0_{IT})_{NAS} - (E_{IT} - E^0_{IT})_{AS}}{s_{AS}} \quad (41)$$

Because $(E_{IT})_{AS} = (E_{IT})_{NAS}$ when equative distribution of the potential for each event is considered, as demonstrated elsewhere [43], and additionally considering $log\beta_{I-L}$ instead of $ln\beta_{I-L}$, Eq. (41) is simplified to:

$$log\beta_{I-L} = \frac{(E^0_{IT})_{AS} - (E^0_{IT})_{NAS}}{s_{AS}\ ln10} \quad (42)$$

4. Results and discussion

4.1. Spectroelectrochemistry measurements with membranes formulated with increasing potassium ionophore/exchanger molar ratio for potassium transfer

Fig. 2 presents the cyclic voltammograms obtained in 10 mM KCl solution with ITO-POT-membrane systems in which the molar ratio between the potassium ionophore (L) and the cation exchanger NaTFPB was varied in the membrane. Specifically, the total amount of NaTFPB (40 mmol kg^{-1}) was kept constant and that of the ionophore was increased to provide 0:40, 10:40, 20:40, 30:40,

40:40 and 80:40 molar ratio of L/NaTFPB (see membrane compositions [M1-M6] in Table S1 in the Supporting Information). Notably, the NaTFPB amount of 40 mmol kg^{-1} was selected from the results obtained in our previous papers [34,43]. As observed, the peak appearing at 367 mV in the 0:40 membrane (Fig. 2a) develops in another peak at 900 mV (Fig. 2b–f) that increased while the former decreased with the ionophore content in the membrane. From previous results, the first peak at 367 mV is attributed to NAS potassium transfer, whereas the peak at 900 mV corresponds to AS potassium transfer with a 1:1 stoichiometry [43].

In addition to these two peaks, there were two other voltammogram features represented as a small peak (or band) at ~600 mV for 10:40, 20:40 and 30:40 L/NaTFPB molar ratios in the membrane; and a shoulder of the peak at 900 mV (AS transfer with 1:1stoichiometry), which is distinguished at about 800 mV for the 20:40 and 30:40 membranes (see the arrows in Fig. 2). The nature of this small peak and shoulder was evaluated with a series of control experiments using the membrane based on a 20:40 L/NaTFPB molar ratio, selected as an intermediate composition. First, we varied the scan rate to confirm that the thin layer behavior of the three peaks, i.e., linear relationship of the peak current against the scan rate, see Fig. S1a in the Supporting Information). Furthermore, the shoulder at ca. 800 mV becomes a better-defined peak (at ca. 750-800 mV) upon lowering the scan rate.

Our core hypothesis is that the peak at 600 mV, but also the shoulder, may likely correspond to AS transfers comprising stoichiometries different than 1:1, which is known to be the most energetically favorable ratio [47]. This behavior indeed agrees with the fundamental theory proposed by Amemiya and co-workers for voltametric ITs at the membrane-sample interface when more than one ion-ionophore stoichiometries are possible [48]. Accordingly, peak distortions in the form of 'localized widenings' were manifested in such a circumstance. The widenings described by Amemiya may indeed appear as 'shoulders' in the peak corresponding to the primary stoichiometry at certain membrane compositions and ion-analyte concentrations. Moreover, the voltametric peak in Fig. 2e for the 40:40 membrane presents this sort of 'local widening' at the peak starting compared to the more symmetrical peak presented by the 80:40 composition (dotted line included in the same figure for a better comparison). This wider peak is likely the result of the peak at 600 mV and the shoulder merging in only one voltammetric wave.

Second, we increased the KCl concentration from 1 to 10 mM and followed any change in the peak position (Fig. S1b in the Supporting Information). Notably, at the lowest KCl concentration, some electrical resistance due to the low background concentration appeared in the voltammogram, i.e., the extra slope at the beginning of the anodic peak. The first peak (at 220 mV, identified as the NAS transfer) was found to shift to more positive potentials: a change of 27 mV when changing the concentration from 1 to 10 mM was observed. This latter magnitude agrees with a sub-Nernstian behavior, which is an expected behavior for the NAS transfer [17,25].

The next peak (ca. 500 mV) shifted to more positive potentials and hence, its association with a possible anion transfer was discarded. Specifically, the peak change was of ca. 90 mV, which is a super-Nernstian magnitude typically found in ionophore-based membranes when the measured concentration is close to the limit of detection [17,49]. This behavior indicated that the peak at 500 mV corresponds to an AS potassium transfer rather than a NAS one. The third peak (at ca. 800 mV and identified as the AS transfer with 1:1 stoichiometry) also shifted to more positive potentials with the KCl concentration in the sample solution: 57 mV from 1 to 10 mM, which corresponds to the expected Nernstian behavior [25,43]. On the other hand, any shift in the shoulder of that peak was not possible to be properly quantified, as observed in Fig. S1b.

Subsequently, we studied the distribution of the charge for each peak (Q_1, Q_2 and Q_3 for the peaks at 367, 600 and 900 mV), but not for the shoulder, at increasing L/NaTFPB molar ratios in the membrane. The results are collected in Table S2 in the Supporting Information. As a general trend, it was observed that the total charge is rather maintained as a result of the integration of a sole peak (membranes M1 and M6 with 0:40 and 80:40 composition) or the addition of the individual charge of each peak appearing in the anodic scan ($Q_1+Q_2+Q_3$ in membranes M2-M5). However, it was not possible to entirely match the total charge (or ion-exchange capacity) in the different membranes because of slight variations in the membrane preparation concerning the weighted amount of the NaTFPB [43]. As a result, the average charge was of 55.9±5.5 μC, with a deviation of less than 10% between the membranes.

With the charge corresponding to each peak and the total charge of the membrane (ion-exchange capacity as the result of $Q_1+Q_2+Q_3$), it is possible to calculate the percentage of charge that is dedicated to the NAS (Q_1) and AS (Q_2+Q_3) transfers of K^+ at each L/NaTFPB molar ratio (Table S2). It is evident how the sum of the AS transfers is favored by the increase of the ionophore in the membrane, being the majority of the charge dedicated to the AS potassium transfers from a 20:40 L/NaTFPB molar ratio (65% for the AS *against* 35% for the NAS). Then, the available charge is entirely dedicated to the AS transfer(s) from a 40:40 L/NaTFPB ratio and the primary 1:1 stoichiometry exclusively appeared for the 80:40 composition, i.e., double molar content of ionophore with respect to the cation exchanger.

Interestingly, the need for a membrane composition based on a double molar content for the ionophore than for the ion exchanger to optimize the ISE response was already reported for potentiometry measurements: The ionophore/exchanger ratio in an ISE membrane was demonstrated to change the potentiometric selectivity by many orders of magnitude [50–54]. The reason for that lies in the stoichiometry of the target ion with the ionophore, which modifies the charge requirements to maintain the electroneutrality in the membrane [9,55,56].

Very recently, the group of Bühlmann has suggested that the presence of two or more complexes of different stoichiometries influences the membrane selectivity, being this only visualized in the potentiometric response when the membrane does not contain an excess of the ionophore with respect to the exchanger [57]. Analogously, our experiments shown that the main (1:1) stoichiometry is exclusively displayed only for the 80:40 ratio, which is indeed the recommended content for potentiometric ISE to show an optimized response. Other stoichiometries –and even NAS transfer– occur when the L/NaTFPB molar ratio decreases, which is in agreement with the theory and experiments proposed by Bühlmann and co-workers [57]. Advantageously, the interrogation of the membrane under a linear sweep potential allows for the visualization of every IT occurring at the sample-membrane interface at increasing ionophore concentrations in contrast to the potentiometric measurements. For future studies, it would be very beneficial to combine both types of theories and experiments: i.e., potentiometry-voltammetry tandem with ISEs.

Another advantage of the voltametric system is that the dynamic conversion of POT to POT^+ upon the applied potential can be monitored by means of spectroelectrochemistry [43]. Absorbance measurements of the POT film at a fix wavelength of 450 nm are combined with the application of a linear sweep potential to the ITO-POT-membrane system, thus providing the dynamic tracing of the oxidized POT^+. Fig. 2 presents normalized dynamic absorbance measurements of the POT film when coupled to the membranes formulated with increasing L/NaTFPB molar ratio (blue lines). For the 0:40 membrane with no ionophore, the absorbance displays one reversible sigmoidal curve in the potential window

from 50 to 600 mV, coinciding with the voltametric peak (Fig. 2a). Moreover, the potential at which the inflection point of the sigmoidal curve appears (311 mV) rather coincides with the peak potential (370 mV).

In the 10:40 membrane (Fig. 2b), the dynamic absorbance splits into two reversible sigmoidal parts with a flat region between them. The two sigmoidal parts (in the ranges of 72–534 mV and 666–1083 mV and with inflection points appearing at 311 and 881 mV) coincide with the two main voltametric peaks at 286 and 927 mV corresponding the NAS and (1:1) AS potassium transfers respectively. Then, the flat region in the absorbance represents that no IT is happening and hence, there is practically no change in the absorbance [43]. However, the small voltammetric peak at 600 mV did not manifest in the dynamic absorbance, likely because a higher resolution of the spectrophotometric measurements would be necessary to be able to visualize such as small peak, which was not actually possible with our experimental setup.

Analogous trend was observed for the 20:40 and 30:40 L/NaTFPB membrane compositions, though the total magnitude for the normalized dynamic absorbance dedicated to either the NAS or (1:1) AS transfers changes with the ionophore concentration in the membrane. Percentages of 73.6, 52.2 and 28.2% were dedicated to the NAS and percentages of 26.4, 47.8 and 71.8% to the AS for the 10:40, 20:40 and 30:40 membrane compositions, respectively. These percentages rather agree with the values calculated for the charge under the NAS and AS voltametric peaks as above discussed (see Table S2). Then, the membranes with 40:40 and 80:40 L/NaTFPB molar ratio, and presenting a single voltammetric peak, displayed a dynamic curve based on a single sigmoidal. More specifically, the potential window is slightly narrower for the 80:40 than for the 40:40 composition (490–1303 mV *versus* 556–1237 mV), as the voltametric peak is also narrower.

Overall, despite the voltammograms reflecting the NAS and AS IT(s) occurring at the membrane-sample interface and the dynamic absorbance exclusively representing the CT in the dynamic conversion of POT to POT^+, our experiments demonstrate the univocal relationship between the CT and the IT(s) in the ITO-POT-membrane system. Indeed, just acquiring the optical data would be enough to describe the system.

As demonstrated in our previous paper, the experimental absorbance related to each membrane composition can be fitted to the mathematical Sigmoidal−Boltzmann model by using Eqs. (43) and (44), depending if the curve presents one or two sigmoidal regions [43]. Moreover, the derivation of those fittings provides the semi-empirical simulation of the corresponding voltammograms by considering Eq. (2) to define the current in the system (theory section).

$$Y = A_2 + \frac{A_1 - A_2}{1 + e^{\left(\frac{x - x_0}{k}\right)}} \tag{43}$$

$$Y = A_3 + \frac{A_1 - A_2}{1 + e^{\left(\frac{x - x_0}{k}\right)}} + \frac{A_2 - A_3}{1 + e^{\left(\frac{x - x_0'}{k'}\right)}} \tag{44}$$

with Y being the $\frac{c_{POT^+}}{c^{Total}_{TFPB^-}}$, A_1, A_2, A_3, x_0, x_0', k and k' fitting parameters, and with x assumed to be equal to the applied potential. Notably, x_0, and x_0' define the inflection points of the sigmoidal transitions, while k and k' determine the slopes of the fitted sigmoidal curve [58].

Fig.3a presents the anodic part of the dynamic absorbance registered at increasing L/NaTFPB molar ratio (solid line) and considering increasing change in absorbance (i.e., inverted direction compared to the data shown in Fig. 2) together with the corresponding fittings using either Eqs. (43) or (44). The parameters used for the fittings are provided in Table 1. As observed, excellent agreement was found between the experimental and the mathematical fittings by the Sigmoidal−Boltzmann model. In addition, it is possible to correlate any of the parameters in the model with a physical meaning of the system under study, as demonstrated in our previous studies [43]. Accordingly, A values are related to the percentage of the $\frac{c_{POT^+}}{c^{Total}_{TFPB^-}}$ ratio (from 0 to 1) that is dedicated to each sigmoidal part in the fitting (i.e., for each IT), x_0 values are ascribed to the standard potential of the related IT, and k relates to the s parameter in the Nernst equation (and therefore to n_{POT}, n_{AS} and n_{NAS}) as defined in the theory section.

Inspecting Table 1 more in detail, x_0 values always coincide with the peak potential of the experimental voltammograms and A_2 values are the same as the charge portion dedicated to the NAS potassium transfer. On the other hand, k values are higher than the Nernstian one (0.059 V) and hence, the associated n is different than the ideal case of $n = 1$. Notably, k values are indeed significantly high in the case of the AS potassium transfer with the different membranes. Therefore, this behavior deserves a special inquiry, as provided in the next section.

The Sigmoidal-Boltzmann fittings can be used to simulate the experimental voltammograms by means of Eq. (2), as presented in Fig. 3b. Peak positions and the normalized charge under the voltametric peaks agreed rather well. Any difference between the simulated and the experimental traces is likely due to the presence of the peak and shoulder at ca. 600 and 700 mV respectively, which are not considered in the mathematical model for simplicity. But also, all the assumptions made in the theory development together with experimental peak asymmetries influenced the results. Advantageously, this is the first time that complex voltametric traces showing ITs of different nature are simulated in such a precise way from experimental measurements of $\frac{c_{POT^+}}{c^{Total}_{TFPB^-}}$, which is uniquely accomplished by spectroelectrochemistry technique.

4.2. Simulation of spectroelectrochemistry measurements with membranes formulated with increasing potassium ionophore/exchanger molar ratio for potassium transfer

Despite the mathematical Sigmoidal-Boltzmann model being useful for the calculation of current profiles showing NAS and AS ITs in the same membrane, this is indeed a semi-empirical approach that needs for the recording of the dynamic absorbance of the POT film. As demonstrated below, this approach is very convenient for the exploration of certain features of the CT−IT system but, pure theoretical calculations by means of the Eqs. (30)–(32) emerge in this paper as a complementary tool to predict both the dynamic absorbance (i.e., gradual oxidation of POT to POT^+) and the current profile at increasing L/NaTFPB molar ratios in the membrane, whatever is the ion and ionophore nature.

Fig. 3c presents the dynamic curves calculated by means of Eqs. (30), (31) or (32) obtained for the analytical solution of $\frac{c_{POT^+}}{c^{Total}_{TFPB^-}}$ in membranes displaying NAS and/or AS IT(s). A comparison with the experimental results can be accomplished by visualization of Fig. 3a *versus* Fig. 3c. At a first glance, the experimental and calculated curves coincide rather well and show similar qualitative trend with increasing ionophore content in the membrane. Notably, only the NAS and the primary AS potassium transfer were selected for the simulation of the curves because the secondary stoichiometries do not manifest properly in the experimental dynamic absorbance, as already discussed.

A deeper evaluation arises when comparing key experimental and calculated parameters of the sigmoidal curves: Table 2 collects the potential window, absorbance change and inflection point for each sigmoidal in both the experimental and calculated curves. As a general trend, the potential window at which each sigmoidal region occurs is always narrower in the calculated curves than in

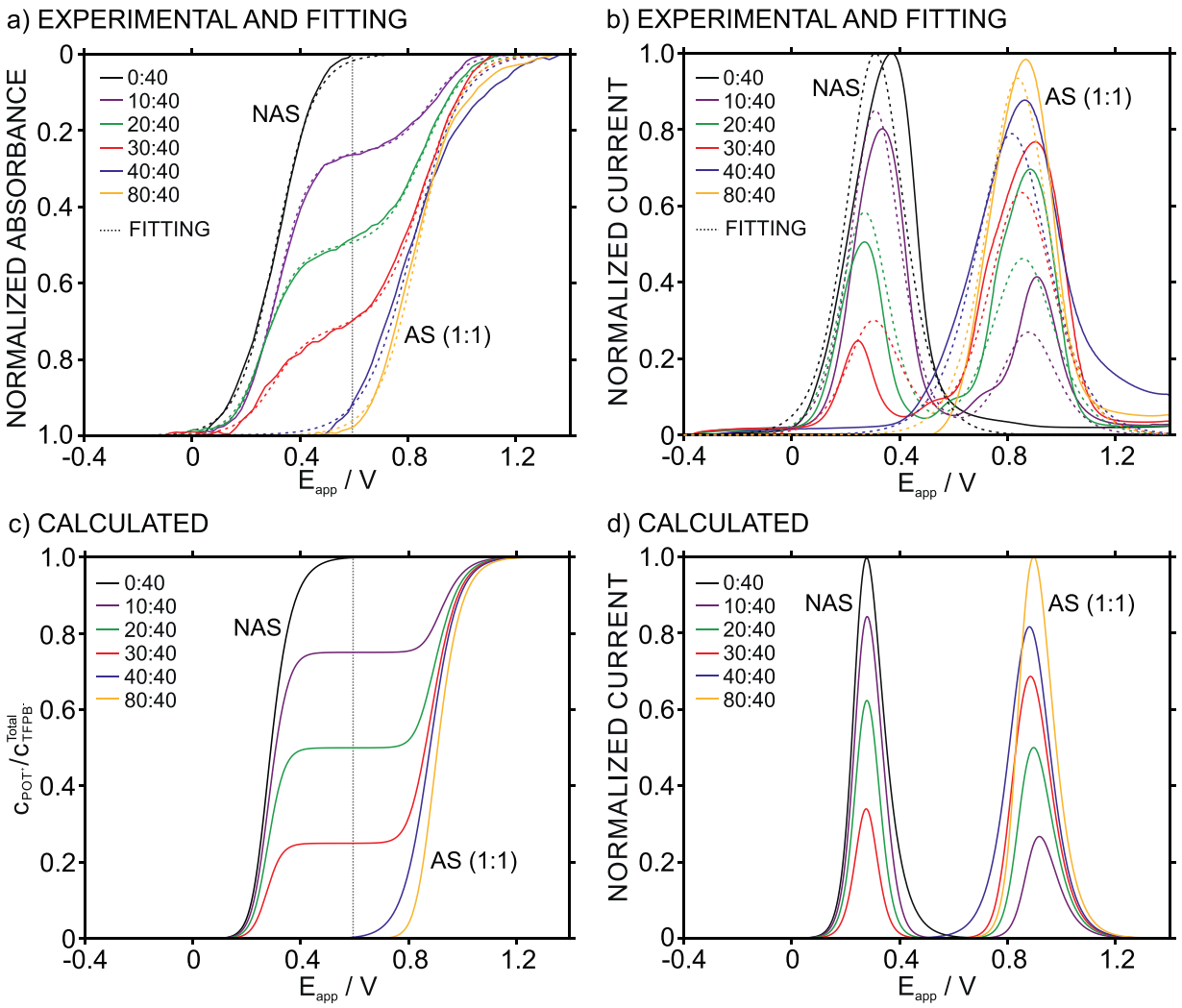

Fig. 3. For 10 mM KCl solution and using increasing potassium ionophore/NaTFPB molar ratios in the membrane: **(a)** Dynamic absorbance corresponding to the anodic part of voltammograms presented in Fig. 2 (solid lines) and the corresponding fittings to the mathematical Sigmoidal-Boltzmann model (dotted lines). **(b)** Experimental anodic peaks (solid lines) and the derivatives of the Sigmoidal-Boltzmann fittings in **(a).** **(c)** Calculated $\frac{c_{POT^+}}{c^{Total}_{TFPB^-}}$ profiles using Eqs. (30)–(32). **(d)** Calculated anodic peaks by means of derivation of the profiles displayed in (c) and using Eq.(2). All the parameters used in the calculations are provided in the Supporting Information. NAS = non-assisted transfer. AS (1:1) = assisted transfer with 1:1 stoichiometry. For interpretation of the references to color in this figure, the reader is referred to the web version of this article.

Table 1
Parameters used for the mathematical fittings of the dynamic absorbance observed with membrane M1-M6 in 10 mM KCl.

		$\frac{c_{POT^+}}{c^{Total}_{TFPB^-}}$ Fittings			Normalized current Fittings		Experimental	
L/NaTFPB	IT nature	*A* values	x_0 values (V)	*k* values (V)	Peak position (V)	charge	Peak position (V)	charge
0:40	NAS	A_1: 0 A_2: 1	x_0: 0.31	*k*: 0.071	0.312	1.00	0.370	1.00
10:40	NAS	A_1: 0	x_0:0.31	*k*: 0.062	0.312	0.74	0.335	0.68
	AS	A_2: 0.74 A_3: 1	x_0': 0.88	*k*': 0.068	0.881	0.26	0.909	0.32
20:40	NAS	A_1: 0	x_0: 0.27	*k*: 0.060	0.271	0.49	0.272	0.38
	AS	A_2: 0.49 A_3: 1	x_0': 0.86	*k*': 0.080	0.861	0.51	0.884	0.62
30:40	NAS	A_1: 0	x_0: 0.30	*k*: 0.066	0.304	0.28	0.246	0.15
	AS	A_2: 0.28 A_3: 1	x_0': 0.85	*k*': 0.081	0.855	0.72	0.904	0.85
40:40	AS	A_1: 0 A_2: 1	x_0: 0.82	*k*: 0.090	0.819	1.00	0.865	1.00
80:40	AS	A_1: 0 A_2: 1	x_0: 0.84	*k*: 0.076	0.841	1.00	0.869	1.00

Table 2
Parameters for the experimental and calculated dynamic normalized absorbance in 10 mM KCl solution and using membranes with increasing potassium ionophore/NaTFPB molar ratio.

		Sigmoidal change(s)						Inflection point		Flat region	
		Exp			Calc			Exp	Calc	Exp	Calc
L/NaTFPB	IT nature	from–to, mV	Absorb %	Slope V^{-1}	from–to, mV	Absorb %	Slope V^{-1}	mV	mV	from–to, mV	from–to, mV
0:40	NAS	50–600	100.0	−3.12	105–581	100.0	−6.18	311	289	–	–
10:40	NAS	72–534	73.6	−2.62	105–496	75.0	−5.31	311	286	534–666	496–763
	AS	666–1083	26.4	-0.86	763–1123	25.0	-1.51	881	927		
20:40	NAS	72–468	51.5	−1.94	105–433	50.0	−3.86	271	275	468–600	433–746
	AS	600–1127	48.5	-1.50	746–1127	50.0	-2.81	860	910		
30:40	NAS	138–500	28.2	−1.00	105–411	25.0	−2.21	304	279	500–600	411–707
	AS	600–1105	71.8	-1.86	707–1141	75.0	-3.98	855	886		
40:40	AS	490–1303	100	−2.27	571–1159	100.0	−4.74	818	865	–	–
80:40	AS	556–1237	100	−2.86	718–1200	100.0	−5.52	840	909	–	–

Table 3
Parameters for the experimental and calculated anodic voltametric peaks observed in 10 mM KCl solution using increasing ionophore/NaTFPB molar ratio in the membrane.

		Peak position, mV			Peak width, mV[a]			Peak charge, norm.[b]		
L/NaTFPB	IT nature	exp	calc	Diff, %	Exp	Calc	Exp/Calc	Exp	calc	Exp/Calc
0:40	NAS	369.8	277.9	20.1	267.7	131.1	2	1.00	1.00	1
10:40	NAS	335.4	279.6	12.8	219.3	121.6	1.8	0.68	0.75	0.9
	AS	908.5	918.6	0.8	182.4	138.0	1.3	0.32	0.25	1.3
20:40	NAS	271.8	278.8	1.8	168.3	108.9	1.5	0.38	0.5	0.8
	AS	884.4	897.5	1.0	250.2	149.3	1.6	0.62	0.5	1.2
30:40	NAS	245.7	276.3	8.3	145.4	98.7	1.5	0.15	0.25	0.6
	AS	903.6	885.1	1.5	319.2	178.9	1.9	0.85	0.75	1.1
40:40	AS	864.9	881.5	1.3	353.0	181.3	2	1.00	1.00	1
80:40	AS	869.1	897.2	2.2	267.0	150.4	1.8	1.00	1.00	1

[a] Width was calculated at half of the peak height. [b] Charge was calculated in voltammograms plotted with normalized values for current.

the experimental ones, while the change in the normalized absorbance (i.e., the c_{POT^+} dedicated to the corresponding IT) agree rather well. This resulted in a slope in the linear range(s) of the sigmoidal part(s) (absorbance change/E_{app}) that is always ~2 times in the calculated curves than in the experimental graphs. Differences also manifested in the flat regions between the different sigmoidal parts, being wider in the calculated than in the experimental curves.

The described differences between the experimental and calculated absorbance curves likely originate from the definition of the equations in the theory section under ideal conditions together with the assumption than only one AS IT (indeed the primary 1:1 stoichiometry) occurs in the membranes. The most interesting feature is the demonstrated dependence of the dynamic $\frac{c_{POT^+}}{c^{Total}_{TFPB^-}}$ with the L/NaTFPB molar ratio in the membrane, which allows a rather accurate prediction of the experimental curves. Indeed, the current profiles can be additionally obtained by derivation of the calculated curves and applying Eq. (2). The calculated voltammetric peaks are displayed in Fig. 3d. While the qualitative trend for the evolution of the calculated peaks at increasing L/NaTFPB ratio evidently agrees with the experiments, there are some remarkably quantitative differences (see Table 3). Comparing first the peak positions, as a general matter, experimental and calculated values agree rather well. Regarding the peak width, the calculated peaks are in average between 1.5 and 2 times narrower than the calculated ones, which directly relates to the narrower potential windows obtained for the calculated sigmoidal curves compared to the experimental ones. Finally, the degrees that the (normalized) charge is dedicated to each IT are quite similar in the calculated and experimental voltammograms.

The main difference between the calculated and experimental anodic voltammograms is the peak width, and thus, this deserves further discussion. As above described, the peak width is a reflection of the potential window at which the POT oxidation occurs in connection with the IT at the membrane-sample interface. Whether it is considered that only one IT is possible, in principle, the isolated POT oxidation can be described using Eqn 6 in the theory section and solving it for the $\frac{c_{POT^+}}{c^{Total}_{TFPB^-}}$ ratio according to Eq. (45). A detailed description on how to reach Eq. (45) in found in the Supporting Information.

$$\frac{c_{POT^+}}{c^{Total}_{TFPB^-}} = \frac{1}{1 + e^{\left(E_{CT} - E^0_{CT}\right)/s_{POT}}} \tag{45}$$

This equation is in the form of the mathematical Sigmoidal−Boltzmann model as per comparison with Eq. (43), with $A_1 = 0$, $A_2 = 1$, $Y = \frac{c_{POT^+}}{c^{Total}_{TFPB^-}}$, $x = E_{CT}$, $x_0 = E^0_{CT}$ and $k = s_{POT}$. Then, $x = E_{app}$ can be assumed, as E_{CT} is a constant fraction of the E_{app}, as described in Eq. (1) in the theory section. The parameter E^0_{CT} is known to be connected with the energy that is needed for the CT-IT event, whereas s_{POT} (equal to $\frac{RT}{n_{POT}F}$) is linked to the total amount of charge that is 'moved' across the interface 1 (Fig. 1a) considering the electroneutrality condition in the CT-IT system [43]. Because such a charge is definitely linked to the width of the voltametric peak, and hence the potential window for the oxidization of POT to POT^+, we have simulated the $\frac{c_{POT^+}}{c^{Total}_{TFPB^-}}$ curves and the corresponding voltammograms at different n_{POT} values (from 0.2 to 1.5, Fig. S2 and Table S3 in the Supporting Information).

Regarding the $\frac{c_{POT^+}}{c^{Total}_{TFPB^-}}$ profiles, all of them were calculated for E_{CT}=0.37 V coinciding with the experimental peak position of the NAS potassium transfer. Then, increasing n_{POT} from 0.2 to 1.5 resulted in narrower potential windows for the sigmoidal, which is translated into narrower voltametric peak simulated by inserting the $\frac{c_{POT^+}}{c^{Total}_{TFPB^-}}$ profiles into Eq. (2). Interestingly, the width that was closer to the experimental voltammogram of the NAS potassium transfer is that corresponding to n_{POT}=0.35 (see Fig. S2c in

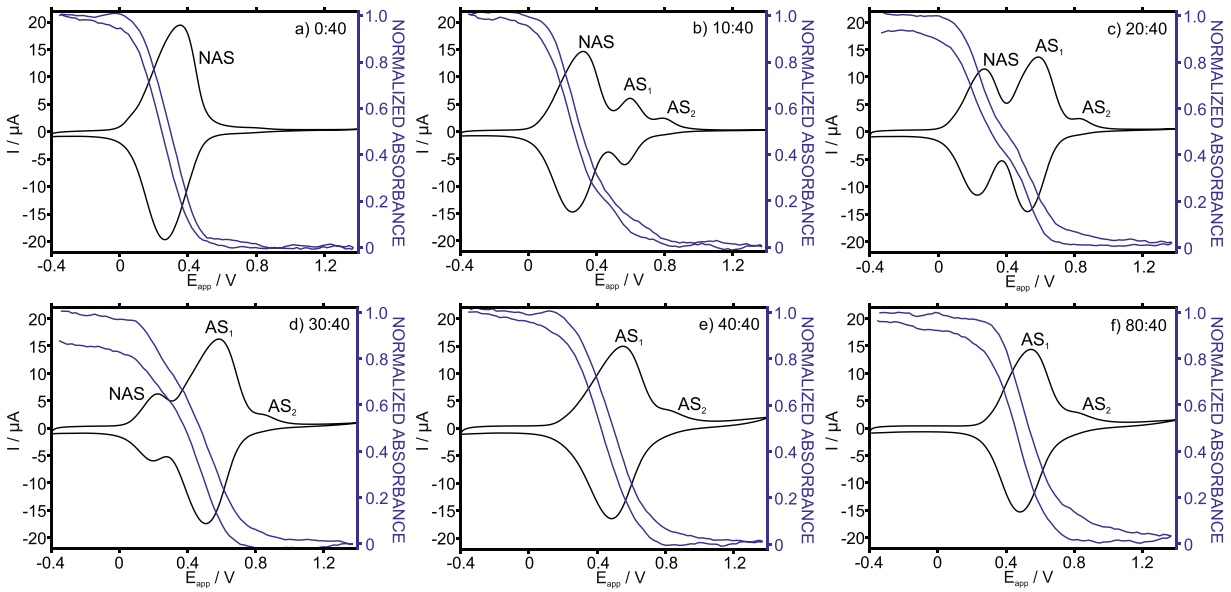

Fig. 4. Voltammograms and dynamic absorbance of the POT film observed in 10 mM NaCl solution with membranes formulated with increasing potassium ionophore/NaTFPB molar ratio: **(a)** 0:40, **(b)** 10:40, **(c)** 20:40, **(d)** 30:40, **(e)** 40:40 and **(f)** 80:40. Scan rate=100 mV s^{-1}. NAS=non-assisted transfer. AS=assisted transfer.

the Supporting Information), therefore confirming that the charge transfer in the ITO-POT-membrane system does not occur through the ideal case of n_{POT}=1. Despite the consideration of non-ideality through n_{POT}=0.35 being easily considered in the equations within the Sigmoidal-Boltzmann model, as just demonstrated, its implementation in the developed theory would be more complex. Changes in the mass balances defining the ITO-POT-membrane system would impede the achievement of any analytical solution, as those obtained for the ideal case (n_{POT}=1). While this direction is possible and would probably provide calculations closer to the experimental curves, this is outside the goal of the present paper.

This later finding is very important to describe the connection between the CT-IT processes. Essentially, the average number of electrons in the material where the CT occurs (in this case the conducting polymer POT, but it could be other material such as redox-active monolayers or metal compounds directly dissolved in the membranes [28–33]) marks the stoichiometry of the IT exchange at the sample-membrane interface. On the other hand, the net charge transfer is limited by the amount of $TFPB^-$ that is present in the membrane and that allows for POT^+ doping upon oxidation. As presented in Fig. S2, the number of electrons involved in the oxidation of the redox active material sets the width of the peaks revealed in the current profile, and this in turn will lead to different levels of peak overlapping additionally depending on the distance between the NAS and AS IT peaks, but whatever displayed in the voltammogram. As a result, to minimize peak overlapping and maximize hence the IT resolution whatever its nature, it would be convenient to have a redox material able to behave under ideal conditions of n = 1. Indeed, an even higher number of electrons would result in a better resolution. This conclusion agrees with previous studies suggesting the use of redox materials different that POT that provides experimental voltammograms slightly narrower than those provided by POT [28].

4.3. Exploring the response of membranes formulated with increasing potassium ionophore/exchanger molar ratio towards a non-preferred cation (sodium, Na^+)

Next, spectroelectrochemistry experiments were performed using the same membranes, formulated with increasing concentrations of the potassium ionophore (M1-M6 in Table 1), but examining a solution that contains a cation different than the primary one for which the ionophore is selective, i.e., sodium instead of potassium. Fig. 4 depicts the cyclic voltammograms and corresponding dynamic absorbance of the POT film in 10 mM NaCl solution. As observed, the membrane with a 0:40 L/NaTFPB molar ratio presented a sole peak at 353 mV with the corresponding dynamic absorbance displaying one sigmoidal curve in the same potential window as the peak and the inflection point rather coinciding with the peak potential (see Tables S4–S6 in the Supporting Information). Furthermore, the results with the 0:40 membrane in NaCl rather coincide with those observed in KCl solution, as the IT is assigned to a NAS one and this is expected to be practically the same for both sodium and potassium ions (according to the Hofmeister series) [25].

As the ionophore content is increased in the membrane, two new peaks appeared at 594 and 793 mV that are in principle ascribed to two different AS sodium transfer, as these peaks appear only when the ionophore is present in the membrane. The peak at 594 mV continues increasing with the ionophore content in the membrane, being clearly the main peak in the voltammograms for 30:40, 40:40 and 80:40 L/NaTFPB molar ratios. On the contrary, the peak at 793 mV did not show any significant trend upon increasing the ionophore concentration in the membrane once it appeared at the 10:40 L/NaTFPB molar ratio. In view of these results, the peak at 594 mV is assigned to the primary 1:1 stoichiometry for the complex between Na^+ and the potassium ionophore, whereas that at 793 mV likely corresponds to a secondary stoichiometry.

Being sodium a non-preferred ion by the ionophore valinomycin, the potential at which the peak related to its primary complex appears at a less positive value than that observed for potassium ion at the same concentration (594 mV *versus* 900 mV). The requirement for a higher potential to generate the IT from the membrane to the solution, according to the mechanism presented in Fig. 1a, is connected to a stronger retention (i.e., binding constant) of potassium over sodium in the membrane, i.e., higher binding constant of the ionophore with potassium than sodium [43]. In other words, peak positions are related to the selectivity profile of the membrane while the level at which this selectivity is manifested in the voltametric response (i.e., NAS and AS ITs) depends on the L/NaTFPB molar ratio in the membrane.

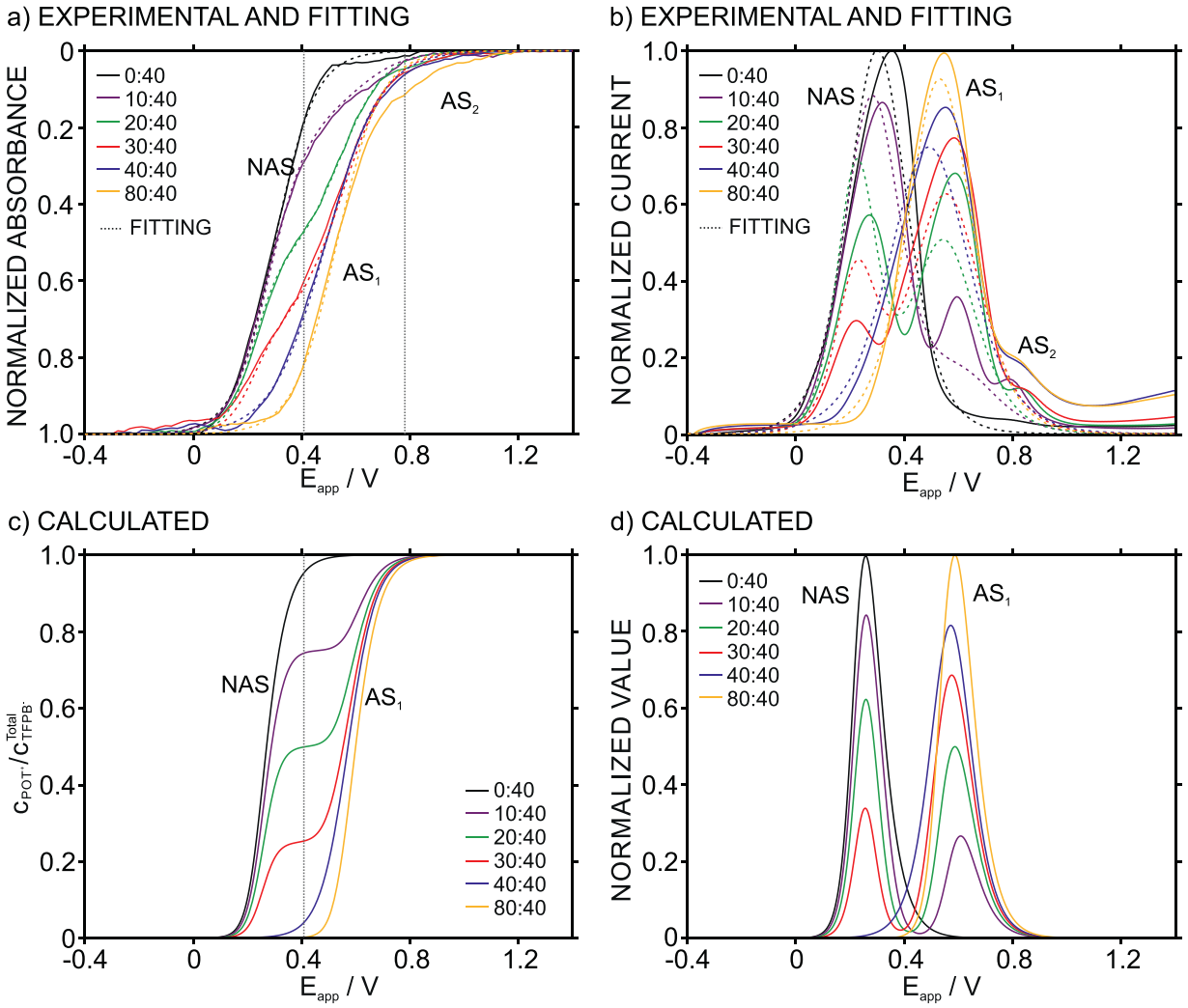

Fig. 5. For 10 mM NaCl solution and using increasing potassium ionophore/NaTFPB molar ratios in the membrane: **(a)** Dynamic absorbance corresponding to the anodic part of voltammograms presented in Fig. 4 (solid lines) and the corresponding fittings to the mathematical Sigmoidal–Boltzmann model (dotted lines). **(b)** Experimental anodic peaks (solid lines) and the derivatives of the Sigmoidal–Boltzmann fittings in **(a). (c)** Calculated $\frac{c_{POT^+}}{c^{Total}_{TFPB^-}}$ profiles using Eqs. (30)–(32). **(d)** Calculated anodic peaks by means of derivation of the profiles displayed in (c) and using Eq. (2). All the parameters used in the calculations are provided in the Supporting Information. NAS=non-assisted transfer. AS=assisted transfer. For interpretation of the references to color in this figure, the reader is referred to the web version of this article.

Other aspect to highlight is the overlapping presented between the NAS and AS sodium transfers, in contrast to the well separated peaks in the case of potassium. This overlapping causes that the transition between the different sigmoidal parts in the experimental dynamic absorbance is vaguely distinguished and flat regions are not even distinguished. As a result, both the Sigmoidal-Boltzmann fittings and the calculated curves by Eqs. (30)–(32) are not matching the experimental results as good as in the case of potassium (Fig. 5, Tables S4–S6). For example, the calculated voltammograms provided peak positions that differ from the experimental ones in an average of 15% for the NAS and < 7% for the AS sodium transfers. Then, and once more, the calculated peak widths are between 1.5–2.0 times narrower than those obtained experimentally, as a result of considering n_{POT}=n_{NAS}=n_{AS}=1. In any case, qualitative trends at increasing L/NaTFPB molar ratio in the membrane totally agree when experimental and calculated curves are compared.

Inspecting now the results for the membranes M1-M6 for the preferred and non-preferred cations in a joint way, it is possible to propose a protocol to establish the selectivity profile in the system on the basis of the different peak positions. Eq. (38) has been developed in the theory section for that purpose, under the assumption that at equal membrane composition and the same concentration of the preferred and non-preferred ions in the solution, the charge dedicated to the IT for the corresponding AS IT is in turn equal. This was confirmed in our experimental results. Table 4 shows the difference between the charge in the AS ITs for potassium (preferred) and sodium (non-preferred) ions with membranes using increasing potassium ionophore/NaTFPB molar ratios. An average difference of 4% was found, which is within the variation percentage found for the total charge variation in different membranes (ca. 10%, see above) associated to preparation reasons (i.e., the weighting process of the membrane components).

Table 4 additionally collects the values of the logarithmic selectivity coefficients using Eq. (38) based on the different positions of the peak potentials. An average $logK_{K,Na}$ value of –5.4±0.4 was obtained, which excellently agrees with those values reported in the literature for analogous membranes interrogated in potentiometry mode (see Table 4) [59–63]. As an alternative of using the voltametric peak potentials, the potential corresponding to the inflection points provided by the fitting of the dynamic absorbance measurements to the mathematical Sigmoidal-Boltzmann model can be used for the calculation of the logarithmic selectivity coefficient. The obtained values are collected in Table 4, with an aver-

Table 4
Calculation of the logarithmic selectivity coefficients by assuming equal charge of the assisted IT for potassium and sodium in membranes formulated with increasing potassium ionophore/NaTFPB molar ratio and using Eq. (38).

L/NaTFPB L=K IP	Voltammograms Diff (%)Q_K–Q_{Na}	$E_{peak,Na} - E_{peak,K}$[a] (V)	$logK_{K,Na}$	Absorbance $E_{inf,Na} - E_{inf,K}$[b](V)	$logK_{K,Na}$	Reported $logK_{K,Na}$ [59, 60][c, d]	[63][e]	[62][f]
10:40	8.7	−0.314	−5.3	−0.271	−4.6	−4.5	−5.1	−4.7
20:40	2.7	−0.293	−4.9	−0.316	−5.3			
30:40	0.1	−0.356	−6.0	−0.301	−5.1			
40:40	5.4	−0.312	−5.3	−0.327	−5.5			
80:40	1.0	−0.324	−5.5	−0.310	−5.2			

[a] Difference between the peak potentials for the assisted IT peaks of Na^+ and K^+ in the voltammograms. [b] Difference between the inflection points for the sigmoidal ascribed to assisted ITs of Na^+ and K^+ in dynamic absorbance curves. [c] Molar ratio of L/exchanger=1:2 for reference [59]. [d] Molar ratio of L/exchanger=4:1 for reference [60]. [e] Molar ratio of L/exchanger=10:1. [f] Molar ratio of L/exchanger=2:1.

Table 5
Calculation of the logarithmic binding constants for different ion-ionophore systems and using Eq. (42).

L/NaTFPB L=K IP	Cation (I)	Voltammograms $E_{peak,AS} - E_{peak,NAS}$[a]	$log\beta_{I-L}$	Absorbance $E_{inf,AS} - E_{inf,NAS}$[b]	$log\beta_{I-L}$	Reported log β_{I-L} I= K^+ [64][c]	[60][d]	[61][c]	I= Na^+ [64][c]	[65][e]
10:40	K^+	0.573	9.71	0.570	9.66	9.32	10.10	10.00	6.65	6.4
	Na^+	0.276	4.68	0.330	5.59					
20:40	K^+	0.613	10.38	0.589	9.98					
	Na^+	0.320	5.42	0.321	5.44					
30:40	K^+	0.658	11.15	0.551	9.34					
	Na^+	0.327	5.54	0.331	4.61					

K IP=potassium ionophore (valinomycin).
[a] Difference between the peak potentials for the assisted and non-assisted IT peaks in the voltammograms. [b] Difference between the inflection points for the sigmoidal ascribed to assisted and non-assisted ITs in dynamic absorbance curves. [c] Molar ratio of L/exchanger=2:1. [d] Molar ratio of L/exchanger=4:1. [e] Molar ratio of L/exchanger=3:4.

age $logK_{K,Na}$ value of −5.1±0.3, again within the range reported in the literature. Thus, it can be concluded that Eq. (38) is suitable to calculate the selectivity coefficients in ITO-POT-membrane systems, with any accuracy deviation ascribed to the assumptions and iterations performed in the theoretical and semiempirical treatments.

The selectivity profile of the membrane reflects the different binding constants for each cation facing the membrane. The magnitude of any ion-ionophore binding constant can be calculated by means of Eq. (42) in the theory section. This later equation utilizes the differences between the E^0 potential of the NAS and AS ITs (i.e., the peak potentials) and has been developed by adapting the theory proposed in our recent publication for membranes independently presenting NAS (no ionophore) and AS (ionophore) transfer of the same ion [43]. Table 5 collects the values calculated for $log\beta_{I-L}$ for I=K^+ and Na^+ from the peak potentials in the voltammograms and the inflection points in the fittings of the dynamic absorbance in the corresponding experiments performed with membranes M2-M4 (L/NATFPB=10:40, 20:40, and 30:40), which show responses to both NAS IT and AS IT. As observed, the $log\beta_{I-L}$ for valinomycin-K^+ complex were calculated to be 10.4±0.7 and 9.7±0.3, given by voltammograms and absorbance curves respectively, both of which agree well with literature values. Lower logarithmic binding constant values were obtained in the case of I=Na^+(5.2±0.5 by voltammograms and 5.5±0.1 by absorbance), which is expected considering the high selectivity of valinomycin towards potassium than sodium ion.

4.4. Prediction of responses, selectivity profiles and binding constants

The mathematical Sigmoidal–Boltzmann model and the developed theory can in principle be jointly utilized to characterize and predict several response characteristics of membranes containing any kind of ionophore and facing any NAS and AS IT at the membrane-sample interface. To demonstrate such a feature, we selected a membrane based on the Na ionophore X in a L/NaTFPB molar ratio of 20:40 (M7), and Na^+ and K^+ as the preferred and non-preferred cations respectively. Fig. 6a and b display the voltammograms and the corresponding dynamic absorbance recorded in 10 mM NaCl and KCl solutions respectively. The NAS IT peaks for Na^+ and K^+ are rather similar regarding peak potentials (305 and 313 mV respectively), while the AS peaks yield a relatively large difference (788 and 601 mV respectively), reflecting a clear preference for sodium over potassium ion. The associated dynamic absorbance curves displayed the typical sigmoidal parts related to each IT, with a flat transition region between them that is more evident in the case of the NaCl solution, as the peak overlapping is lower than in the KCl solution.

Subsequently, we predicted the $\frac{c_{POT^+}}{c^{Total}_{TFPB^-}}$ profiles of Na^+ and K^+ NAS and AS ITs with membranes containing increasing Na ionophore/NaTFPB molar ratios, using the peak potentials in Fig. 6a and b as $(E^0_{IT})_{NAS}$ and $(E^0_{IT})_{AS}$ for Na^+ and K^+ and using Eq. (32). The simulated curves (Fig. 6c and d) are plotted together with the fitting of the experimental curves (dotted line) to the mathematical Sigmoidal-Boltzmann model for comparison, with the corresponding parameters collected in Tables S7–S9 in the Supporting Information. Moreover, these curves were transformed into current profiles through Eq. (2) and the corresponding results are depicted in Fig. 6e and f after normalization (for the used parameters see Tables S10 and S11 in the Supporting Information). Once more, the main difference between calculated and experimental curves (and hence fittings to the mathematical model) originates from the peak width, as the simulated peaks are ca. 2 times wider than the experimental ones. Regarding peak positions, the predicted AS peak potentials are really close to the experimental values (1.4% and 0.3% difference for NaCl and KCl respectively), whereas the NAS peaks displayed slightly higher difference (11% and 8% for NaCl and KCl respectively). Overall, the qualitive features of the prediction are in excellent agreement with the experimental data.

As above introduced for the valinomycin-based membrane, the AS IT potential difference between Na^+ and K^+ can be further utilized to calculate the selectivity coefficient of the ionophore. Analogously, Table S12 collects the calculated values for $logK_{K,Na}$ as

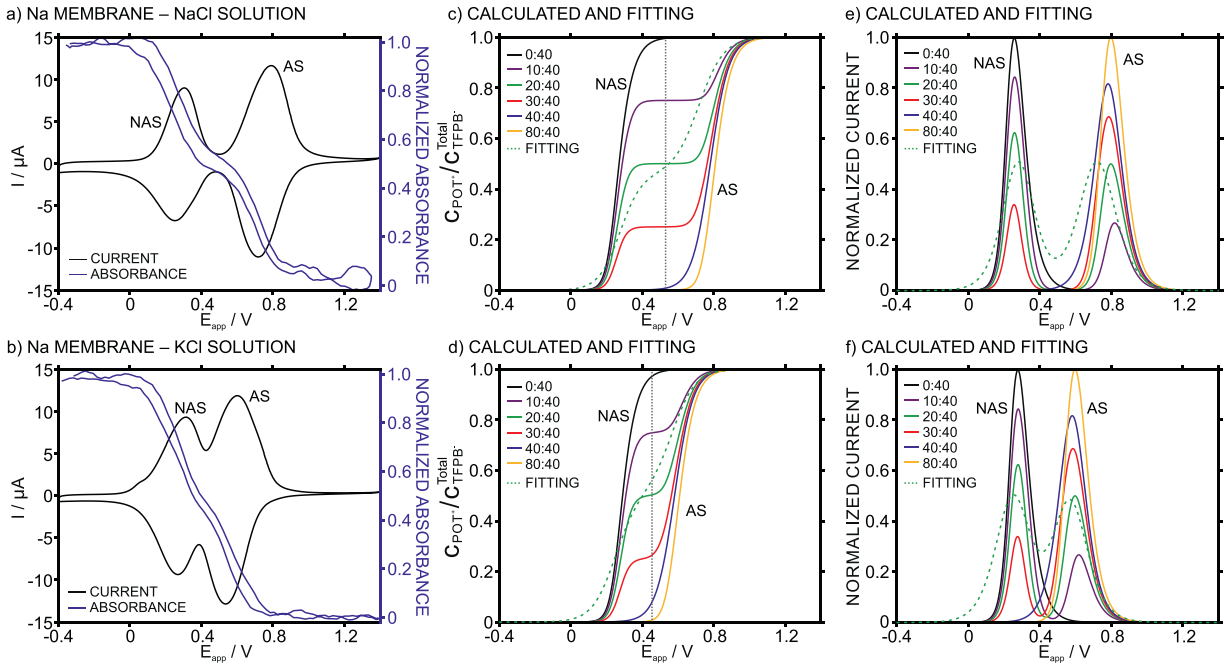

Fig. 6. For a membrane with 20:40 molar ratio of sodium ionophore/NaTFPB: Experimental voltammograms and dynamic absorbance of the POT film in **(a)** 10 mM NaCl and **(b)** 10 mM KCl solution. Calculated $\frac{C_{POT^+}}{C^{Total}_{TFPB^-}}$ profiles using Eqs. (30)–(32) for membranes containing increasing L/NaTFPB molar ratios in **(c)** 10 mM NaCl and **(d)** 10 mM KCl solution. Fitting of the experimental curve to the mathematical Sigmoidal-Boltzmann model is provided with dotted lines. **(e)** Calculated anodic peaks by means of derivation of the profiles displayed in **(c)** and using Eq. (2). **(f)** Calculated anodic peaks by means of derivation of the profiles displayed in **(d)** and using Eq. (2). All the parameters used in the calculations and fittings are provided in the Supporting Information. Scan rate=100 mV s^{-1}. NAS=non-assisted transfer. AS=assisted transfer. For interpretation of the references to color in this figure, the reader is referred to the web version of this article.

well as those reported in the literature. From the voltammetric peaks and the dynamic absorbance, the logarithmic selectivity coefficients are calculated to be −3.16 and −2.52 respectively, with the latter one being even closer to the range reported in the literature (from −2.0 to −2.5). This agreement confirms again the feasibility of using the developed method to calculate the membrane selectivity coefficients.

Binding constants $log\beta_{I-L}$ for the Na ionophore were also determined and values are reported in Table S13. For I = Na^+, the calculated $log\beta_{I-L}$ values of 8.17 (from voltammograms) and 7.46 (from absorbance) highly agree with the previously reported value of ca. 7.6 in literature [60,61,63,64]. Weaker binding strength was observed with the sodium ionophore-K^+ complex, as the $log\beta_{I-L}$ is calculated to be 4.93 from voltammetry and 5.42 from optical measurement, coinciding with the already reported value 4.8 [64].

Overall, with the developed theory, it is possible to predict the current profiles at different L/NaTFPB molar ratios in the membrane together with the estimation of selectivity coefficients and binding constants. It is only necessary to experimentally obtain the $(E^0_{IT})_{NAS}$ and $(E^0_{IT})_{AS}$, which could be achieved by a single experiment using a membrane with a 20:40 L/NaTFPB molar ratio, but it could be whatever presenting the NAS and AS transfer of the studied ion. In addition, the difference of this potential values could be used whether binding constant values already reported in the literature are used into the developed theory. This opens up further research in the direction of predicting voltammetric responses for multi-ionophore membranes backside contacted with new redox materials (with at least n=1), accelerating hence the provision of new electrodes for multi-ion detection with optimized selectivity profiles and peaks' resolution (i.e., minimum overlapping).

5. Conclusions

Spectroelectrochemistry technique has demonstrated to be an essential tool to provide tangible evidence of the dynamic charge-transfer (CT) process in redox active films of poly(3-octylthiophene) (POT) that are interconnected with ultrathin ion-selective membrane that facilitates different number and nature of ion transfers (ITs). In particular, the application of an anodic linear sweep potential gradually oxidizes POT to POT^+, which results in a series of ITs at the membrane-sample interface driven by electroneutrality requirements. Each IT is manifested in an individual voltammetric peak, whereas the CT in the POT film is monitored through a dynamic absorbance profile. Specifically, the ITs are of non-assisted and assisted nature when different molar ratios of the ionophore and the ion-exchanger compound are utilized in the membrane. The observed experimental behavior is well-predicted by a theory formulated on the basis of the definition of each interface of the CT-IT system: at increasing ionophore concentration in the membrane, the assisted IT associated to the primary ion-ionophore stoichiometry (1:1 in our case) acquires importance through the dedicated charge in the voltammetric peak. The theory can be indistinctly utilized for ions with a different preference level by the ionophore, which additionally permits evaluating the selectivity profile of the POT-membrane system. Overall, the developed theory well complement with the use of the mathematical Sigmoidal−Boltzmann for the fittings of the experimental dynamic absorbance observed in the POT film and describing hence the CT-IT process in a highly complete manner. Calculated voltammograms well agree with the experimental data, whereas ion-ionophore binding constants can be also estimated, showing excellent correlation with values previously reported in the literature. Advantageously, new findings about the number of electrons associated to the CT in the POT material may facilitate further investigations in maximizing peak resolution in the voltammetric experiments. The developed theory may undoubtedly help as the basis of future research towards new electrodes for multi-ion detection with optimized features through the prediction of the peak overlapping level when several ionophores are simultaneously present in the membrane.

Declaration of Competing Interest

The authors declare that they have no known competing financial interests or personal relationships that could have appeared to influence the work reported in this paper.

Credit authorship contribution statement

Yujie Liu: Methodology, Software, Validation, Formal analysis, Investigation, Data curation, Writing - original draft, Visualization. **Gaston A. Crespo:** Conceptualization, Formal analysis, Resources, Writing - original draft, Supervision, Funding acquisition. **Maria Cuartero:** Conceptualization, Methodology, Formal analysis, Resources, Writing - original draft, Visualization, Supervision, Project administration, Funding acquisition.

Aknowledgments

This project has received funding from the European Research Council (ERC) under the European Union's Horizon 2020 research and innovation programme (grant agreement No. 851957). Y.L. gratefully thanks the China Scholarship Council for supporting her Ph.D. studies.

Supplementary materials

Supplementary material associated with this article can be found, in the online version, at doi:10.1016/j.electacta.2021.138634.

References

[1] J. Bobacka, A. Ivaska, A. Lewenstam, Potentiometric ion sensors, Chem. Rev. 108 (2008) 329–351.
[2] M. Cuartero, M. Parrilla, G.A. Crespo, Wearable potentiometric sensors for medical applications, Sensors 19 (2019) 363.
[3] J.J. García-Guzmán, C. Pérez-Ràfols, M. Cuartero, G.A. Crespo, Microneedle based electrochemical (bio) sensing: towards decentralized and continuous health status monitoring, TrAC Trends Anal. Chem. (2020) 116148.
[4] M. Cuartero, G.A. Crespo, All-solid-state potentiometric sensors: a new wave for in situ aquatic research, Curr. Opin. Electrochem. 10 (2018) 98–106.
[5] T. Guinovart, M. Parrilla, G.A. Crespo, F.X. Rius, F.J. Andrade, Potentiometric sensors using cotton yarns, carbon nanotubes and polymeric membranes, Analyst 138 (2013) 5208–5215.
[6] M. Novell, M. Parrilla, G.n.A. Crespo, F.X. Rius, F.J. Andrade, Paper-based ion-selective potentiometric sensors, Anal. Chem. 84 (2012) 4695–4702.
[7] G.A. Crespo, S. Macho, F.X. Rius, Ion-selective electrodes using carbon nanotubes as ion-to-electron transducers, Anal. Chem. 80 (2008) 1316–1322.
[8] M. Cuartero, J.S. del Río, P. Blondeau, J.A. Ortuño, F.X. Rius, F.J. Andrade, Rubber-based substrates modified with carbon nanotubes inks to build flexible electrochemical sensors, Anal. Chim. Acta 827 (2014) 95–102.
[9] E. Bakker, P. Bühlmann, E. Pretsch, The phase-boundary potential model, Talanta 63 (2004) 3–20.
[10] X.U. Zou, J.H. Cheong, B.J. Taitt, P. Bühlmann, Solid contact ion-selective electrodes with a well-controlled Co (II)/Co (III) redox buffer layer, Anal. Chem. 85 (2013) 9350–9355.
[11] E. Jaworska, M.L. Naitana, E. Stelmach, G. Pomarico, M. Wojciechowski, E. Bulska, K. Maksymiuk, R. Paolesse, A. Michalska, Introducing cobalt (II) porphyrin/cobalt (III) corrole containing transducers for improved potential reproducibility and performance of all-solid-state ion-selective electrodes, Anal. Chemistry 89 (2017) 7107–7114.
[12] J. Hu, A. Stein, P. Bühlmann, Rational design of all-solid-state ion-selective electrodes and reference electrodes, TrAC Trends in Analytical Chemistry 76 (2016) 102–114.
[13] U. Vanamo, J. Bobacka, Instrument-free control of the standard potential of potentiometric solid-contact ion-selective electrodes by short-circuiting with a conventional reference electrode, Analytical chemistry 86 (2014) 10540–10545.
[14] T. Sokalski, A. Ceresa, M. Fibbioli, T. Zwickl, E. Bakker, E. Pretsch, Lowering the detection limit of solvent polymeric ion-selective membrane electrodes. 2. Influence of composition of sample and internal electrolyte solution, Analytical Chemistry 71 (1999) 1210–1214.
[15] T. Sokalski, A. Ceresa, T. Zwickl, E. Pretsch, Large improvement of the lower detection limit of ion-selective polymer membrane electrodes, Journal of the American Chemical Society 119 (1997) 11347–11348.
[16] L. Höfler, I. Bedlechowicz, T. Vigassy, R.E. Gyurcsányi, E. Bakker, E. Pretsch, Limitations of current polarization for lowering the detection limit of potentiometric polymeric membrane sensors, Analytical chemistry 81 (2009) 3592–3599.
[17] M. Cuartero, J. Ortuno, M. Garcia, G. Sanchez, M. Mas-Montoya, D. Curiel, Benzodipyrrole derivates as new ionophores for anion-selective electrodes: Improving potentiometric selectivity towards divalent anions, Talanta 85 (2011) 1876–1881.
[18] L. Lvova, D. Monti, C.D. Natale, R. Paolesse, The long-lasting story of one sensor development: from novel ionophore design toward the sensor selectivity modeling and lifetime improvement, Sensors 21 (2021) 1401.
[19] S. Suman, R. Singh, Anion selective electrodes: a brief compilation, Microchem. J. 149 (2019) 104045.
[20] G.A. Crespo, E. Bakker, Dynamic electrochemistry with ionophore based ion-selective membranes, RSC Adv. 3 (2013) 25461–25474.
[21] Y. Kim, P.J. Rodgers, R. Ishimatsu, S. Amemiya, Subnanomolar ion detection by stripping voltammetry with solid-supported thin polymeric membrane, Anal. Chem. 81 (2009) 7262–7270.
[22] P. Si, E. Bakker, Thin layer electrochemical extraction of non-redoxactive cations with an anion-exchanging conducting polymer overlaid with a selective membrane, Chem. Commun. (2009) 5260–5262.
[23] B. Kabagambe, A. Izadyar, S. Amemiya, Stripping voltammetry of nanomolar potassium and ammonium ions using a valinomycin-doped double-polymer electrode, Anal. Chem. 84 (2012) 7979–7986.
[24] A.R. Harris, J. Zhang, R.W. Cattrall, A.M. Bond, Applications of voltammetric ion selective electrodes to complex matrices, Anal. Methods 5 (2013) 3840–3852.
[25] G.n.A. Crespo, M. Cuartero, E. Bakker, Thin layer ionophore-based membrane for multianalyte ion activity detection, Anal. Chem. 87 (2015) 7729–7737.
[26] D. Yuan, M. Cuartero, G.A. Crespo, E. Bakker, Voltammetric thin-layer ionophore-based films: part 1. Experimental evidence and numerical simulations, Anal. Chem. 89 (2017) 586–594.
[27] J. Zhang, A.R. Harris, R.W. Cattrall, A.M. Bond, Voltammetric ion-selective electrodes for the selective determination of cations and anions, Anal. Chem. 82 (2010) 1624–1633.
[28] M. Cuartero, L. Chai, B. Zhang, R. De Marco, G.A. Crespo, Ferrocene self assembled monolayer as a redox mediator for triggering ion transfer across nanometer-sized membranes, Electrochim. Acta 315 (2019) 84–93.
[29] Y. Yang, M. Cuartero, V.R. Gonçales, J.J. Gooding, E. Bakker, Light-addressable ion sensing for real-time monitoring of extracellular potassium, Angew. Chem. Int. Ed. 57 (2018) 16801–16805.
[30] M. Cuartero, R.G. Acres, J. Bradley, Z. Jarolimova, L. Wang, E. Bakker, G.A. Crespo, R. De Marco, Electrochemical mechanism of ferrocene-based redox molecules in thin film membrane electrodes, Electrochim. Acta 238 (2017) 357–367.
[31] S. Jansod, L. Wang, M. Cuartero, E. Bakker, Electrochemical ion transfer mediated by a lipophilic Os (ii)/Os (iii) dinonyl bipyridyl probe incorporated in thin film membranes, Chem. Commun. 53 (2017) 10757–10760.
[32] Z. Jarolímová, J. Bosson, G.M. Labrador, J. Lacour, E. Bakker, Ion transfer voltammetry at thin films based on functionalized cationic [6]helicenes, Electroanalysis 30 (2018) 650–657.
[33] Z. Jarolímová, J. Bosson, G.M. Labrador, J. Lacour, E. Bakker, Ion transfer voltammetry in polyurethane thin films based on functionalised cationic [6]helicenes for Carbonate detection, Electroanalysis 30 (2018) 1378–1385.
[34] M. Cuartero, G.A. Crespo, E. Bakker, Ionophore-based voltammetric ion activity sensing with thin layer membranes, Anal. Chem. 88 (2016) 1654–1660.
[35] M. Cuartero, G.A. Crespo, E. Bakker, Polyurethane ionophore-based thin layer membranes for voltammetric ion activity sensing, Anal. Chem. 88 (2016) 5649–5654.
[36] K. Xu, G.A. Crespo, M. Cuartero, Subnanomolar detection of ions using thin voltammetric membranes with reduced Exchange capacity, Sens. Actuators B Chem. 321 (2020) 128453.
[37] K. Xu, M. Cuartero, G.A. Crespo, Lowering the limit of detection of ion-selective membranes backside contacted with a film of poly (3-octylthiophene), Sens. Actuators B Chem. 297 (2019) 126781.
[38] M.B. Garada, B. Kabagambe, Y. Kim, S. Amemiya, Ion-transfer voltammetry of perfluoroalkanesulfonates and perfluoroalkanecarboxylates: picomolar detection limit and high lipophilicity, Anal. Chem. 86 (2014) 11230–11237.
[39] T. Han, Z. Mousavi, U. Mattinen, J. Bobacka, Coulometric response characteristics of solid contact ion-selective electrodes for divalent cations, J. Solid State Electrochem. 24 (2020) 2975–2983.
[40] P.J. Greenawalt, S. Amemiya, Voltammetric mechanism of multiion detection with thin ionophore-based polymeric membrane, Anal. Chem. 88 (2016) 5827–5834.
[41] R. Ishimatsu, A. Izadyar, B. Kabagambe, Y. Kim, J. Kim, S. Amemiya, Electrochemical mechanism of ion-ionophore recognition at plasticized polymer membrane/water interfaces, J. Am. Chem. Soc. 133 (2011) 16300–16308.
[42] C. Mao, D. Yuan, L. Wang, E. Bakker, Separating boundary potential changes at thin solid contact ion transfer voltammetric membrane electrodes, J. Electroanal. Chem. 880 (2021) 114800.
[43] Y. Liu, A. Wiorek, G.A. Crespo, M. Cuartero, Spectroelectrochemical evidence of interconnected charge and ion transfer in ultrathin membranes modulated by a redox conducting polymer, Anal. Chem. 92 (2020) 14085–14093.
[44] D. Yuan, M. Cuartero, G.A. Crespo, E. Bakker, Voltammetric thin-layer ionophore-based films: part 2. semi-empirical treatment, Anal. Chem. 89 (2017) 595–602.
[45] A. Wiorek, M. Cuartero, R. De Marco, G.A. Crespo, Polyaniline films as electrochemical-proton pump for acidification of thin layer samples, Anal. Chem. 91 (2019) 14951–14959.
[46] E. Bakker, Selectivity of liquid membrane ion-selective electrodes, Electroanalysis 9 (1997) 7–12.

[47] M.M. Shultz, O.K. Stefanova, S.B. Mokrov, K.N. Mikhelson, Potentiometric estimation of the stability constants of ion-ionophore complexes in ion-selective membranes by the sandwich membrane method: theory, advantages, and limitations, Anal. Chem. 74 (2002) 510–517.
[48] P.J. Greenawalt, M.B. Garada, S. Amemiya, Voltammetric characterization of ion-ionophore complexation using thin polymeric membranes: asymmetric thin-layer responses, Anal. Chem. 87 (2015) 8564–8572.
[49] Z. Szigeti, T. Vigassy, E. Bakker, E. Pretsch, Approaches to improving the lower detection limit of polymeric membrane ion-selective electrodes, Electroanal. Int. J. Devot. Fundam. Pract. Asp. Electroanal. 18 (2006) 1254–1265.
[50] P. Meier, W. Morf, M. Läubli, W. Simon, Evaluation of the optimum composition of neutral-carrier membrane electrodes with incorporated cation-exchanger sites, Anal. Chim. Acta 156 (1984) 1–8.
[51] D. Ammann, E. Pretsch, W. Simon, E. Lindner, A. Bezegh, E. Pungor, Lipophilic salts as membrane additives and their influence on the properties of macro-and micro-electrodes based on neutral carriers, Anal. Chim. Acta 171 (1985) 119–129.
[52] R. Eugster, P.M. Gehrig, W.E. Morf, U.E. Spichiger, W. Simon, Selectivity-modifying influence of anionic sites in neutral-carrier-based membrane electrodes, Anal. Chem. 63 (1991) 2285–2289.
[53] U. Schaller, E. Bakker, U.E. Spichiger, E. Pretsch, Ionic additives for ion-selective electrodes based on electrically charged carriers, Anal. Chem. 66 (1994) 391–398.
[54] S. Amemiya, P. Bühlmann, E. Pretsch, B. Rusterholz, Y. Umezawa, Cationic or anionic sites? Selectivity optimization of ion-selective electrodes based on charged ionophores, Anal. Chem. 72 (2000) 1618–1631.
[55] E. Bakker, P. Bühlmann, E. Pretsch, Carrier-based ion-selective electrodes and bulk optodes. 1. general characteristics, Chem. Rev. 97 (1997) 3083–3132.
[56] P. Bühlmann, L.D. Chen, Ion-selective electrodes with ionophore-doped sensing membranes, Supramol. Chem. From Mol. Nanomater. 5 (2012) 2539–2580.
[57] I. Yilmaz, L.D. Chen, X.V. Chen, E.L. Anderson, R.C. Da Costa, J.A. Gladysz, P. Buhlmann, Potentiometric selectivities of ionophore-doped ion-selective membranes: Concurrent presence of primary ion or interfering ion complexes of multiple stoichiometries, Anal. Chem. 91 (2019) 2409–2417.
[58] M. Rahaman, A. Aldalbahi, P. Govindasami, N.P. Khanam, S. Bhandari, P. Feng, T. Altalhi, A new insight in determining the percolation threshold of electrical conductivity for extrinsically conducting polymer composites through different sigmoidal models, Polymers 9 (2017) 527.
[59] E. Bakker, Determination of improved selectivity coefficients of polymer membrane ion-selective electrodes by conditioning with a discriminated ion, J. Electrochem. Soc. 143 (1996) L83.
[60] Y. Qin, Y. Mi, E. Bakker, Determination of complex formation constants of 18 neutral alkali and alkaline earth metal ionophores in poly (vinyl chloride) sensing membranes plasticized with bis (2-ethylhexyl) sebacate and o-nitrophenyloctylether, Anal. Chim. Acta 421 (2000) 207–220.
[61] Y. Mi, E. Bakker, Determination of complex formation constants of lipophilic neutral ionophores in solvent polymeric membranes with segmented sandwich membranes, Anal. Chem. 71 (1999) 5279–5287.
[62] F. Criscuolo, I.N. Hanitra, S. Aiassa, I. Taurino, N. Oliva, S. Carrara, G. De Micheli, Wearable multifunctional sweat-sensing system for efficient healthcare monitoring, Sens. Actuators B Chem. 328 (2021) 129017.
[63] J. Bobacka, A. Ivaska, A. Lewenstam, Plasticizer-free all-solid-state potassium-selective electrode based on poly (3-octylthiophene) and valinomycin, Anal. Chim. Acta 385 (1999) 195–202.
[64] E. Bakker, E. Pretsch, Ion-Selective electrodes based on two competitive ionophores for determining effective stability constants of ion– carrier complexes in solvent polymeric membranes, Anal. Chem. 70 (1998) 295–302.
[65] E. Bakker, M. Willer, M. Lerchi, K. Seiler, E. Pretsch, Determination of complex formation constants of neutral cation-selective ionophores in solvent polymeric membranes, Anal. Chem. 66 (1994) 516–521.